The Cryosphere Discuss., doi:10.5194/tc-2016-116, 2016
Manuscript under review for journal The Cryosphere
Published: 16 June 2016

The Cryosphere Discussions
Open Access
EGU

Incorporating Distributed Debris Thickness in a Glacio-Hydrological Model: Khumbu Himalaya, Nepal.

James S. Douglas[1], Matthias Huss[2,3], Darrel A. Swift[1], Julie M. Jones[1], Franco Salerno[4,5]

[1] Department of Geography, University of Sheffield, Sheffield, UK.
[2] Department of Geosciences, University of Fribourg, CH-1700 Fribourg, Switzerland.
[3] Laboratory of Hydraulics, Hydrology and Glaciology, ETH Zurich, Zurich, Switzerland.
[4] National Research Council, Water Research Institute, Brugherio (IRSA -CNR), Italy.
[5] Ev-K2-CNR Committee, Via San Bernardino, 145, Bergamo 24126, Italy.

Correspondence to: James S. Douglas* (JDouglas1@sheffield.ac.uk)

Abstract. Understanding the future evolution of Himalayan glaciers is important in terms of runoff that provides an essential water source to local populations and has far-reaching downstream impacts. However, the climatic response of glaciers in High-Mountain Asia is complicated by ice stagnation and considerable supraglacial debris coverage, which insulates the ice from warming. Typical runoff modelling only crudely incorporates debris cover and there is currently no consensus on how significantly this may impact future glacier and runoff evolution. Here, a glacio-hydrological model is modified to incorporate fully distributed debris cover, using melt reduction factors that vary depending on debris thickness, and to redistribute mass losses according to observed surface elevation changes. A range of debris thickness data are implemented, including a remote-sensing survey and a modelled debris surface, to analyse the sensitivity of glacier evolution and runoff to possible future debris-cover changes in a series of experiments in the upper Khumbu catchment, Nepal. Simulations are undertaken using climate input data from Regional Climate Model simulations from CORDEX (Coordinated Regional Downscaling Experiment) which are further statistically downscaled using data from the Pyramid meteorological station. Results suggest that the accurate calibration of the model to volume change compensates for the inclusion of distributed debris cover but only if the climatic sensitivity of the calibration period (1999-2010) and the nature of the debris-covered surface remain constant during future simulations. Altering the nature of the debris surface has a significant impact on simulated ice volume, with melt rates under debris suppressed by up to 85 %. The sensitivity of runoff ranges from 60 to 140 million m^3 yr^{-1}, although there are considerable uncertainties relating to non-glacial snow melt. Moreover, incorporating locally enhanced melt at ice cliffs into the model also impacts upon volume loss and discharge, with a greater proportion of ice cliffs leading to enhanced volume losses compared to a homogeneous debris surface. Finally, using the most representative model configuration, the future evolution of Khumbu Glacier under various climate scenarios shows continued mass losses with a reduction in volume ranging from 60 % to 97 % by 2100. Runoff trends show an initial increase followed by an eventual decrease, with runoff in 2100 predicted to be 8 % lower than current levels.

Keywords: Glacier, Runoff, Debris, Bias Correction, Himalaya

1 Introduction.

The hydrological systems of the Himalayas are vitally important to very large populations in the surrounding countries (Akhtar et al., 2008; Kehrwald et al., 2008). At the source of many catchments, high elevation glaciers and snow represent an important freshwater store that provides river discharges outside of the monsoon season (Immerzeel et al., 2013). Changes in this water storage can therefore have a significant impact on water availability that can subsequently affect agriculture, drinking water and hydropower downstream (Xu et al., 2009). Moreover, glacier mass loss has been shown to increase the

The Cryosphere Discuss., doi:10.5194/tc-2016-116, 2016
Manuscript under review for journal The Cryosphere
Published: 16 June 2016

frequency of Glacier Lake Outburst Floods (GLOFs; Thakuri et al., 2015; Worni et al., 2013; Benn et al., 2012; Bolch et al., 2008).

The level of understanding of catchments in high-mountain Asia is limited and has only recently received much scientific attention. Significant limitations in data monitoring, access, and the difficulties of working at high altitude mean considerable barriers still exist. A specific problem is limited knowledge of the future response of glaciers to climate change, particularly considering that a high proportion (36 % in the Everest region; Thakuri et al., 2014) of Himalayan glaciers are highly debris covered (Scherler et al., 2011). This complicates their climatic response, with surface lowering and stagnation dominating over frontal recession (Benn et al., 2012; Quincey et al., 2009). Such mass loss and downwasting promotes thickening and expansion of debris due to exposure of buried englacial debris and limited debris transport to proglacial areas (Rowan et al., 2015; Anderson, 2000).

Several studies have investigated the impacts of debris upon melt rates (Ragettli et al., 2015; Rounce et al., 2015; Fyffe et al., 2014; Nicholson and Benn, 2013). However, recent approaches have focussed on energy balance approaches, which perform well but require significant in-situ data limiting their wide-spread application. Other studies have modelled the evolution of the debris surface. For example, Rowan et al. (2015) applied a coupled ice-flow mass-balance model to the Khumbu Glacier to determine the long-term glacier response to debris cover, finding that debris cover encourages surface lowering and prolongs the glacier's response to climate change. Shea et al. (2015) simulated glacier changes in the Everest region using a mass-balance and ice-redistribution model, finding sustained mass loss in the 21st century.

In terms of runoff, regional studies have shown that climate changes do affect these high-elevation catchments (Immerzeel et al., 2010). However, the response is not spatially uniform and the impacts are less clear than other regions, for example, the European Alps, since the summer melt peak coincides with the peak in monsoon rainfall (Immerzeel et al., 2013; Miller et al., 2012). More localised studies of upper catchments have shown a strong glacier contribution to runoff, particularly outside of the monsoon season (Thayyen et al., 2007), but this is highly scale dependent, with impacts on the large downstream rivers, for example the Ganges, likely to be minor (Miller et al., 2012). Although there are several recent studies focussing on specific aspects of Himalayan glaciers, for example, ice-cliffs and supraglacial ponds (Miles et al., 2016; Steiner et al., 2015; Sakai et al., 2000), debris-surface energy balance (Collier et al. 2015; Rounce et al., 2015; Fujita & Sakai 2014), and stagnation (Quincey et al., 2009), there has been limited attention on how significant these elements are for impact studies. For instance, it is not yet clear whether incorporating distributed debris cover and stagnation into hydrological models will influence runoff projections.

Here, the influence of debris cover on runoff is investigated by implementing the Glacier Evolution and Runoff Model (GERM; Huss et al., 2008b) to the Khumbu Glacier, Nepal. The model is modified to incorporate spatially variable debris thickness, with melt rates adjusted depending on debris depth. Because the true thickness and future behaviour of the debris is unknown, several model configurations, using various debris thicknesses and parameter groups, are designed to provide the full range of uncertainty concerning debris thickness and melt rates. These debris surfaces include simulated debris thickness distribution of Rowan et al. (2015) and remote-sensing based debris thickness observations of Rounce and McKinney (2014). To investigate the impact of debris inclusion, the model is used in its original form, with no consideration of debris, as well as in its modified form, with debris included, thus allowing one to assess whether the model more realistically simulates runoff when debris is included or ignored. Care is taken to retain the portable nature of the model so that is can easily be implemented in a range of catchments. The simulations of future glacier changes are forced with output from Regional Climate Models (RCMs) from the Coordinated Regional Downscaling Experiment (CORDEX). Due to the complex topography of the region, further statistical downscaling is required, and here we apply the quantile mapping approach of Piani et al. (2010).

The Cryosphere Discuss., doi:10.5194/tc-2016-116, 2016
Manuscript under review for journal The Cryosphere
Published: 16 June 2016

2 Study Area and Data.

The Khumbu catchment (136 km^2) (close to Pheriche: 27.88° N, 86.82° E; Fig. 1) is located on the southern slopes of Mt. Everest (eastern part of central Himalaya) in the Sagarmatha (Everest) National Park (SNP), extending from an elevation of 4200 to 8848 m a.s.l.. The two glaciers (Khumbu, and Changri) occupy 44 km^2, or 32% of the catchment. These glaciers are identified as summer-accumulation glaciers that are fed mainly by summer precipitation from the South Asian monsoon system (Ageta and Fujita, 1996). Recently, Thakuri et al. (2014) traced the surface area loss and Snow Line (SL) altitudinal shift of glaciers in the SNP since the early 1960s. These authors show that the SL shifted ca. +327 m and +232 m, respectively for Khumbu, and Changri Glacier, suggesting these glaciers have experienced a consistent negative mass balance since the 1960s, manifested in downwasting processes, as is typical for debris-covered glaciers (e.g. Bolch et al., 2011).

Direct glaciological data on Khumbu Glacier is limited to short-term mass balance surveys (Inoue, 1977) and ice thickness estimates (Gades et al. 2000; Moribayashi, 1978). Since long-term data are desirable for model calibration, geodetic mass balance is used in this study, for example, Gardelle et al. (2013) reports the specific mass loss of Khumbu and Changri Glaciers from 1999-2010 to be -0.51 and -0.42 m w.e. yr^{-1}, respectively. Table 1 summarises available data and includes several recent geodetic surveys, indicating broad agreement on the rates of mass loss. Glacier outlines are provided by the Randolph Glacier Inventory version 3 (Pfeffer et al., 2014) and the Shuttle Radar Topography Mission (SRTM) provides elevation data.

Both the Khumbu and Changri Glaciers exhibit significant debris cover (37% and 24% of total glacier surface, respectively), particularly in the lower sections where ice flow has stagnated with surface velocities of less than 10 m yr^{-1} (Quincey et al., 2009). More active ice (up to 80 m yr^{-1}) exists immediately downslope of the Khumbu ice fall limiting debris accumulation in this area. Estimating debris thicknesses for large areas is extremely difficult due to the highly heterogeneous nature of the surface and the difficulties accessing and measuring debris depth. Therefore, in this study, a range of surfaces are implemented to investigate the full range of debris estimates. Firstly, the modelled debris surface of Rowan et al. (2015; 100 m resolution) is used to provide an upper bound for debris thickness, with average debris thickness of 147 cm and a standard deviation of 40 cm. Secondly, Rounce and McKinney (2014) used a remote-sensing-based (30 m resolution) approach to survey debris thickness, implemented here to provide a lower bound for debris thickness, with an average depth of 15 cm and a standard deviation of 11 cm. More details on debris surfaces can be found in Sect. 3.3.2.

Meteorological data are available from the Pyramid meteorological station (27.959° N, 86.813° E, 5035 m a.s.l.) located on the lateral moraine of Khumbu (Fig. 1). Salerno et al. (2015) extended this dataset thus providing a continuous daily record from 1994-2013, using neighbouring stations to fill gaps within the data. These data indicate that the climate is characterised by summer monsoons, with a prevailing S-N direction (Ichiyanagi et al., 2007). During the last twenty years, the total annual accumulated precipitation is 446 mm yr^{-1}, with a mean annual temperature of -2.45 °C. In total, 90% of the precipitation is concentrated during June-September.

Very limited long-term discharge measurements are available for the high-elevation catchment. For this study, discharge data from a hydrometric station at Pheriche owned by the Italian research institute, IRSA-CNR, are used. Corresponding discharges are calculated using a stage-discharge curve developed during 2012-2014 via field surveys (using flow tracking, and salt tracers).

The Cryosphere Discuss., doi:10.5194/tc-2016-116, 2016
Manuscript under review for journal The Cryosphere
Published: 16 June 2016

3 Methods.

3.1. Climate Time Series.

GCM (Global Climate Model) outputs cannot be directly used to force local-scale models without prior correction (Piani et al., 2010; Sharma et al., 2007). Therefore, this study utilises RCM simulations from the state-of-the-art CORDEX downscaling experiment (50 km resolution; CORDEX, 2015), which are further downscaled using a quantile-mapping statistical approach, based on the methods of Piani et al. (2010). This approach requires *evaluation* simulations (forced by ERA-Interim reanalysis data) as well as *future* simulations forced by GCM simulations of Representative Concentration Pathways (RCPs 2.6, 4.5, 8.5 - see van Vuuren et al. (2011) for details) to ensure various future emissions scenarios are included (Taylor et al. 2007).

The bias correction procedure is applied to simulations from two RCMs. Firstly, the Rossby Centre Regional Atmospheric Model (RCA4) developed by the Swedish Meteorological and Hydrological Institute (Samuelsson et al., 2011). The simulations used are driven by the ICHEC-EC-EARCH (Irish Centre for High-End Computing) GCM, for RCP 2.6, 4.5 and 8.5. Secondly, REMO (REgional atmosphere MOdel developed by the Max-Planck-Institut für Meteorologie; Jacob, 2009; Jacob and Podzun, 1997) is applied. The simulations used are driven by the Nor-ESM (Norwegian Earth System Model) GCM for RCP 4.5 and 8.5. These were the two simulations available that included evaluation simulations at the time of writing.

3.1.1. Correction of Meteorological Data.

The daily precipitation data monitored at 5035 m a.s.l. as reported by Salerno et al. (2015) for the 1994-2013 period was further processed to correct for potential gauge-undercatch using the approach outlined in Yang et al. (1998) using wind speed and gauge height. Thus, the final corrected precipitation time-series provides a more accurate record of winter accumulation where solid precipitation was likely underestimated (Salerno et al., 2015; Fig. S1).

3.1.2. Bias Correction of Regional Climate Models.

The quantile-mapping technique of Piani et al. (2010) is implemented since it adjusts for both the mean and variability of the simulated data by matching the intensity distributions of the observations. Additionally, it removes overestimation of 'drizzle' days, a known limitation of daily GCM and RCM precipitation (Piani et al., 2010).

The correction for precipitation assumes that both the observed and simulated distributions are described by the gamma distribution. For precipitation corrections, the monthly Cumulative Distribution Functions (CDFs) and the number of dry days of the simulated and observed variables are calculated. A transfer function, $y=f(x)$, where y is corrected precipitation and x is simulated precipitation, is then computed as:

$$CDF_{\text{obs}}\big(f(x)\big) = CDF_{\text{sim}}(x) \quad (1)$$

This transfer function can then be used to apply the difference between the simulated and observed distributions to future precipitation data series. For temperature, the same approach is taken except the normal distribution is used to calculate the CDF. The results of these corrections for the observation period are included in Fig. S2. Crucially, this method uses the evaluation CORDEX-South Asia simulations together with the longest available meteorological record (1994-2012) to constrain the correction.

To ensure the bias correction is robust, the corrections were independently cross-validated by dividing the time-series of observations and simulations in two; 1994-2002 was 'training' data to calculate the parameters of the distribution transfer

The Cryosphere Discuss., doi:10.5194/tc-2016-116, 2016
Manuscript under review for journal The Cryosphere
Published: 16 June 2016

function, and 2003-2010 was treated as 'validation' data to which the correction was applied. This process was then reversed and the results compared using evaluation metrics (root-mean-square error and absolute error) to ensure the correction functioned over periods with no observations. To test whether the correction is accurately reproducing conditions that cause the onset of melt, the onset of the melt season (>5 consecutive warm days) is calculated. For precipitation, the annual dry day frequency is calculated to assess the reproduction of rainfall frequency and removal of drizzle. Results of the cross-validation and metrics are presented in Sect. 4.1. For the final bias correction for application to the model, the full duration of the meteorological data are used.

3.1.3. Future Climate Scenarios.

There are two main sources of error affecting simulations: RCM bias, caused by factors such as topography, which is addressed by bias correction; and GCM bias, which is inherited from the GCM through its boundary conditions (Kotlarski et al., 2014), caused by inaccurate monsoon representation, for example. Evaluation simulations are forced by reanalysis data so contain only the RCM bias. However, historical simulations are forced with CMIP5 boundary conditions so contain both RCM and GCM bias. The bias correction outlined here corrects evaluation simulations using observations, therefore removes the RCM bias. When applied to historical and RCP simulations, the RCM bias is again removed, only the GCM bias now remains.

This bias was identified in this study as a temperature offset between the end of evaluation simulations and the beginning of future scenarios during the overlap period of 2006-2010 (Fig. S3), with no offset evident in the precipitation simulations. Not correcting this bias would impose a false warming of around 1 °C so modifications must be made to the bias correction methodology. With abundant model simulations, the solution could be to use the GCM with the smallest offset. However, due to limited simulations and the large errors of available GCMs, the solution here is to use the mean of historical temperature simulations in the bias correction, with the standard deviation of the evaluation simulations. This ensures the bias-corrected temperature in future scenarios is related to the calibration period, yet the variability is still constrained by evaluation simulations since this most accurately reproduces observed conditions.

3.2. Glacier-Evolution and Runoff Model (GERM).

GERM is a fully distributed glacio-hydrological model designed for highly glacierised catchments capable of calculating components of the water balance at high resolutions (daily and 50 m) and has been well proven in the European Alps and Central Asia (Sorg et al., 2014; Farinotti et al., 2012; Huss et al., 2008b). This highly-parameterised model is portable in that its input requirements are limited to daily temperature and precipitation and a digital elevation model of the glacier surface, but its applicability to Himalayan catchments is untested. A brief overview of GERM will follow, while a full description can be found in Huss et al. (2008b) and Farinotti et al. (2012). GERM consists of five modules to represent accumulation, ablation, glacier evolution, evaporation and runoff routing.

Glacier mass balance is calculated using the accumulation and ablation modules. Precipitation is classed as snow if the temperature is below 1.5°C with a linear transition range of ±1°C. Ablation of snow and ice is calculated using a distributed temperature-index model that is enhanced to also include potential solar radiation (Hock, 1999):

$$M = \begin{cases} \left(f_M + r_{ice/snow} \cdot I_{pot,i}\right).T_i & : \mathrm{T} > 0°\mathrm{C}: \\ 0 & : \mathrm{T} \leq 0°\mathrm{C}: \end{cases} \quad (2)$$

The Cryosphere Discuss., doi:10.5194/tc-2016-116, 2016
Manuscript under review for journal The Cryosphere
Published: 16 June 2016

where f_M is a degree day factor, $r_{ice/snow}$ are separate radiation factors for snow and ice, $I_{pot,i}$ is the potential direct clear-sky radiation at grid cell i, and T_i is the mean daily air temperature at the same location. T is interpolated using a constant lapse rate. Seasonal snow cover in non-glacial areas melts in the same way as snow in glacial areas until no snow remains.

The runoff module of GERM is summarised here and fully explained in Farinotti et al. (2012). Runoff is routed through a suite of fast and slow linear storage reservoirs depending on the surface type. Due to the nature of the Khumbu catchment, only three surface types are distinguished: ice, snow, rock. The local water balance is solved at all grid cells:

$$Q_i = P_{liq,i} + M_i - ET_i - \sum_r \Delta v_{r,i}, \quad (3)$$

where Q_i is the runoff at day i, P_{liq} is liquid precipitation, M_i is melt from the ablation module, ET is evapotranspiration and ΔV is the storage change of the reservoir, r. Potential ET is calculated based on the air temperature, saturation vapour pressure, surface type and daylight per day (Huss et al., 2008). Areas outside of the glacial mask are treated in the same way as glacial areas, with the surface type dictating which runoff reservoir is active. Finally, the total catchment discharge is computed as the sum of Q_i for all grid cells.

3.2.1. Glacier Recession and Stagnation.

Glacier evolution is calculated using a mass-conserving Δh-parameterisation, fully described in Huss et al. (2010) and used in a range of studies (e.g. Huss & Hock, 2015; Li et al., 2015; Farinotti et al., 2012). This parameterisation redistributes annual volume change over the ice surface according to typical patterns of mass losses from observations and has been shown to result in glacier surface evolution similar to more complex ice flow modelling. Since these spatial patterns of mass loss were not based on debris-covered glaciers, the appropriateness of using these 'typical' curves is questionable (Huss et al., 2010). Therefore, a glacier-specific parameterisation was developed for Khumbu, based on the elevation changes found by Nuimura et al. (2012) for the period 1992-2008. This curve dictates that mass changes are relatively homogeneously distributed over the lower two thirds of the glacier, rather than focussing on the terminus region as is typical for most receding glaciers (Fig. 2). This pattern of mass redistribution mimics the patterns of mass loss observed in numerous geodetic mass balance surveys for debris-covered glaciers in the Everest region (Gardelle et al., 2013; Nuimura et al., 2012; Bolch et al., 2011) and is applied to all model configurations.

3.2.2. Initial Ice Volume.

Accurate estimates of initial ice volume and thickness are important to ensure that simulated future volume changes are reliable (Huss et al., 2014). This study uses a combination of modelling and interpolation to calculate bed geometry and thickness. Gades et al. (2000) conducted a series of radio-echo sounding transects on the lower section of Khumbu (Fig. 1), which are used as ground control points to interpolate the bed. This is combined with modelled thickness where data are not available using the methods of Huss and Farinotti (2012) who estimate ice thickness from an inversion of surface topography based on glacier mass turnover and ice flow dynamics. Specifically, the surface mass balance distribution is estimated and used to calculate the ice flux volume, which is converted into ice thickness using the ice flow law (Glen, 1955). This thickness distribution (Fig. 1) and volume compares well to those used by Rowan et al. (2015) who employ a similar methodology. Finally, to evaluate the modelled ice thickness in areas without independent thickness data, the purely-modelled thickness is compared to observed thickness. The results of this show an oversteepening of the bed in the purely-modelled topography, resulting in erroneously thin ice beneath (-40 m) the icefall and thick ice near the terminus (+50 m).

The Cryosphere Discuss., doi:10.5194/tc-2016-116, 2016
Manuscript under review for journal The Cryosphere
Published: 16 June 2016

Although these errors are removed when the control points are interpolated for ice beneath the icefall, they provide an indication of the uncertainty associated with areas of the glacier that have no independent ice thickness observations.

3.2.3. Distributed Debris Cover.

Supraglacial debris cover can perturb the melt rate of ice (Østrem, 1959) by reducing the albedo of ice from typical values of 0.25-0.5 to values of 0.1 (Cuffey and Paterson, 2010), which increases the absorption of incoming radiation. If the debris layer is sufficiently thin (<3 cm), this energy flux will be conducted to the ice surface causing enhanced surface melting (Nicholson and Benn, 2006). However, studies in the Himalayas suggest that the impact of thin debris at the glacier-scale is negligible due to limited coverage of *thin* debris, so it is not included here (Pratap et al., 2015; Inoue and Yoshida, 1980). Instead, the dominant influence of debris on Himalayan glaciers is an insulating effect. Specifically, a thicker layer of debris (>3 cm) will result in reduced melt compared to bare ice, since the debris absorbs incoming radiation during the day and returns this energy to the atmosphere at night, preventing efficient transmission to the ice (Nicholson and Benn, 2013).

In this study, rather than using a constant reduction factor, the effect of distributed debris cover has been incorporated into GERM by adding a thickness-dependent reduction factor, f_{debris}, which applies once seasonal snow cover has melted:

If T > 0°C and debris covered: $$M = \left(\left(f_M + r_{ice} \,.\, I_{pot,i}\right).T_i\right).f_{\text{debris}} \quad (4)$$

$$f_{\text{debris}} = e(c.D_t) \quad (5)$$

where f_{debris} is the correction factor of debris-covered ice, e is the exponential constant, and c is the coefficient that describes the shape of the melt reduction curve depending on debris thickness, D_t. This melt reduction curve is based on the observed melt rates under debris from the nearby Ngozumpa Glacier whereby melt rates under 50 cm of debris are 50 % of surface melt rates (Nicholson and Benn, 2006). Thus, the model now calculates surface melt using a fully distributed melt-correction depending on the thickness of surface debris. Debris thickness data is described in Sect. 3.3.2.

Debris-covered ice also encourages the formation of ice cliffs (Hambrey et al., 2009) where ablation can be strongly enhanced locally (Reid and Brock, 2014; Sakai et al., 2000) due to exposed low-albedo ice, aspect (Sakai et al., 1998), and the transfer of atmospheric energy into the glacier interior through melt-pond drainage (Miles et al., 2016; Steiner et al., 2015). Thus, in areas defined as ice cliffs (see Sect. 3.3.2), melt is modified such that it is equal to the bare-ice melt rate by assigning ice-cliff areas a debris thickness value of 0 cm.

3.3. Model Configurations.

3.3.1. Model Configuration for Calibration Period (1999-2010).

The lack of long-term glaciological data is a key limitation to calibration. Without direct mass balance measurements, geodetic mass balance can be used. This is an excellent indicator of glacier response to climate since it integrates the entire glacier and provides the water volume lost (Jost et al., 2012). However, it does not yield information on precipitation so care must be taken to ensure the correct volume change is not simulated, for example, by underestimating melt and underestimating precipitation to compensate. Of the geodetic surveys summarised in Table 1, the time period covered by the data set of Gardelle et al. (2013) best fits with the duration of meteorological data. Moreover, the observed mass balance of -0.51 m w.e. yr^{-1} from 1999-2010, sits between those of Bolch et al. (2011) and Nuimura et al. (2012).

To calibrate GERM, simulations were initiated from 1999-2010 with the ablation parameters (f_M, r_{ice}, r_{snow}) adjusted separately until simulated mass balance matched the mass balance from Gardelle et al. (2013) of -0.51 m w.e. yr^{-1}. The accumulation parameter group was not altered during this process since meteorological input data was adjusted externally to

The Cryosphere Discuss., doi:10.5194/tc-2016-116, 2016
Manuscript under review for journal The Cryosphere
Published: 16 June 2016

correct for gauge-undercatch and the precipitation lapse rate was taken from observations of Salerno et al. (2015), thus constraining these parameters allowing reasonable calibration of the ablation parameters. The ablation parameters were tuned by systematically altering the parameters by ±10 % until the modelled mass balance most closely reproduced observed mass balance, with the ratio between the three ablation parameters (f_M, r_{ice}, r_{snow}) kept constant. Bias-corrected RCM outputs were used to drive the model during this period. This was preferred to in-situ meteorological data in order to ensure continuity with of future glacier behaviour.

In order to investigate the impact of debris inclusion on glacier and runoff evolution, the calibration is performed using the original model (ignoring debris) and with a thick debris layer, resulting in two separate calibration configurations and two separate parameter groups: *bare ice parameters* and *debris parameters*. These parameter sets provide the minimum (bare ice) and maximum (debris) bounds for debris depth and thus melt parameters. The modelled volume change has to reproduce the independent observed volume change in each separate configuration, yet the addition of a debris surface inhibits melt. Therefore, the melt parameters must compensate for the debris layer in order to simulate observed volume changes. This is explained schematically in Fig. 3.

3.3.2. Debris Surfaces.

The aforementioned *bare ice* is taken directly from the digital elevation model. The thick debris surface used in calibration is produced in Rowan et al. (2015) by modelling the evolution of the debris surface, hereafter referred to as *thick debris*. This *thick debris* surface is less variable than reality, so should be considered an upper-bound for the reduction of melt under debris.

Although a thick debris surface is expected to protect the ice surface from rapid melt (Rowan et al., 2015), the impact of ice cliffs and supraglacial lakes are not fully understood (e.g. Thakuri et al., 2015). To test whether ice cliffs can have a destabilising influence on glacier response, a variety of alternate debris layers are used (Fig. 4, and Table 2) in addition to the thick debris surface of Rowan et al. (2015). Firstly, the debris surface of Rowan et al. (2015) is modified to include the size and locations of ice cliffs. This layer, *thick debris with ice cliffs*, uses the locations and size of melt-ponds as a proxy for ice cliffs (Ragettli et al., 2015; Zhang et al., 2011), with debris thickness altered to zero. Melt pond data from Watson et al. (in review) provides pond outlines for Khumbu Glacier. Secondly, the ice-cliff layer is further modified to mimic continued growth of ice cliffs and disintegration of the debris surface, producing the *thick debris with increased ice cliffs* surface. Finally, the *thin debris* surface is from the remote-sensing based study of Rounce and McKinney (2014) providing a thin, highly heterogeneous surface.

3.3.3. Model Configurations for Future Simulations.

To explore the sensitivity of glacier evolution and runoff to supraglacial debris, a series of model configurations are used implementing several combinations of parameter sets and debris surfaces. The configurations are designed to provide a comprehensive assessment of the sensitivity of the model to debris cover. Figure 5 demonstrates the calibration process and how the parameter groups and debris surfaces are applied in *configurations 1-4* for future simulations. All configurations employ the same retreat-parameterisation curve developed specifically for Khumbu (Sect. 3.2.1).

Configuration 1 represents implementation of GERM with no knowledge of debris cover, i.e. the calibration parameter set was parameterised with a bare-ice surface, and the future simulation contains no reduction factor for debris surfaces. Since this is a continuation of the calibration configuration for bare ice, it is therefore expected to produce realistic future volume changes. *Configuration 2* uses the same bare-ice parameter sets, but this configuration adds the thick debris surface

The Cryosphere Discuss., doi:10.5194/tc-2016-116, 2016
Manuscript under review for journal The Cryosphere
Published: 16 June 2016

of Rowan et al. (2015) for future simulations, so melt is reduced depending on debris thickness. Thus, the differences between *configurations 1* and 2 *isolate* the influence of the thick debris surface.

Configuration 3 uses the parameter set calculated when thick debris was applied during calibration, but does not apply debris in the future simulations, therefore mimicking the effect of total debris removal. This demonstrates the extent to which ice may melt without debris, providing an upper bound for the sensitivity analysis. C*onfiguration 4A* uses the debris cover parameter set with the thick debris surface for future simulations. Thus, it is a continuation of the calibration configuration so is expected to produce realistic future volume changes. *Configurations 4B-D* apply the alternate debris surfaces (see Table 2) in future simulations, used to test the impact of ice cliffs on future glacier response.

These configurations are designed to provide the full-range of uncertainty associated with debris thickness since the true nature of the surface, as well as its future evolution, are unknown. *Configurations 1-4A* all implement either *bare ice* or *thick debris*, whereas *configurations 4B-D* implement alternate debris surfaces.

3.4. Experiments.

The model configurations are grouped into experiments where each comparison will explore a different aspect of model sensitivity:

- **Experiment 1:** *configurations 1* and *4* are compared. These 'calibrated' simulations use the same model configuration as the calibration period, thus simulating reasonable runoff projections.
- **Experiment 2:** *configurations 2* and *3 are compared.* This provides a sensitivity analysis exploring the difference in runoff when the model is modified after the calibration.
- **Experiment 3:** sensitivity analysis exploring the impact of ice cliffs and melt ponds on runoff, using the *configurations 4A-D.* By using constant calibration parameters, the differences between each configuration isolate the effects of the choice of debris-surface.

3.5. Model Simulations of Future Glacier Evolution.

In addition to the aforementioned experiments, simulations employing the most realistic model configuration are performed using simulations from two RCMs for three RCPs to explore the future evolution of runoff at Khumbu. To determine the most realistic configuration, discharge data from Pheriche are used to resolve whether the *bare ice configuration* or the *debris configuration* most accurately reproduces observed discharge (see Sect. 4.4).

4 Results.

4.1. Bias Correction Evaluation and Future Climate Scenarios.

Table 3 shows the results of the cross-validation bias correction evaluation metrics, demonstrating considerable improvements to the original RCM outputs. The independent cross-validation performs equally well compared to the full bias correction, suggesting the methodology is robust. Figure 6 shows the bias-corrected future temperature and precipitation of RCA4 and REMO for the three RCPs (see Fig. S4 for trend analysis). All scenarios show warming over the 21st century; however, REMO simulations suggest more considerable decadal variability compared to RCA4. For RCP 4.5, mean temperature increase averaged across RCA4 and REMO is 0.012°C yr^{-1}, compared to 0.034°C yr^{-1} and 0.003°C yr^{-1} for RCP 8.5 and 2.6 respectively. Precipitation trends are less clear (Fig. S4). RCA4 scenarios show significant ($P<0.05$) negative trends for RCP 4.5 and 8.5 whereas REMO RCP 4.5 shows a significant ($P<0.05$) positive trend. It should be emphasised

The Cryosphere Discuss., doi:10.5194/tc-2016-116, 2016
Manuscript under review for journal The Cryosphere
Published: 16 June 2016

that, although every care has been taken to ensure this process uses the best available data and techniques, the limitations of sparse monitoring networks and limited availability of CORDEX-South Asia model outputs, the projections presented here are not to be considered best estimates of future glacier change.

4.2. Calibration Results.

GERM was calibrated separately for two configurations (with and without debris) as described in Sect. 3.3.1, producing the parameter sets in Table 4. Both these parameter sets reproduce observed geodetic mass balances from 1999-2010 of -0.51 m w.e. yr^{-1} for their respective configurations. Figure 7 shows the closely matched mass balance and near-identical volume changes during the calibration period. Validation of the model outputs using the alternative geodetic studies shown in Fig. 7 is difficult, since the timing of the studies coincides yet the estimated mass balances are different. Moreover, the uncertainty range of Bolch et al. (2011) and Nuimura et al. (2012) are both ±0.52 m w.e. yr^{-1}.

4.3. Experimental Results:

4.3.1. Experiment 1: Calibrated Simulations.

The two model *configurations (1*- without debris, and *4*- with thick debris cover*)* for which calibration to volume change took place show minimal differences in overall future glacier volume loss, glacier shrinkage and mass balance (Fig. 8 and 9). For example, considering the entire glacier, the remaining ice volume of *configuration 1* by 2100 is 28.2 %, whereas *configuration 4A* is 28.4 %, compared to 2010. In the case of bare ice (*configuration 1*), the relative melt factors are low so the sensitivity of bare ice melt to temperature change is relatively small. Conversely, with thick debris (*configuration 4A*), relative melt factors are high, so there is more melt with warming, yet the insulating effect of the debris balances this to produce very similar overall glacier response with strongly reduced mass loss in the lower ablation area, but higher mass loss above the debris-covered tongue. Since both configurations use the Khumbu-specific retreat parameterisation, the spatial pattern of mass loss is very similar (Fig. 9). Experiments 2 and 3 will assess how sensitive model outputs are to the assumption of debris changes by altering the nature of the debris surface.

4.3.2. Experiment 2: Model Sensitivity.

There is a substantial difference in the rate of volume loss between *configurations 2* and *3*, with *configuration 2* (low melt parameters with thick debris surface) showing limited volume loss compared to *configuration 3* (high melt parameters with no debris), as shown in Fig. 8. The regions with mass loss in Fig. 9 reflect this pattern with Fig, 9b showing minor changes whereas Fig. 9c shows dramatic ice loss beneath the ice fall, highlighting the influence of the debris on glacier evolution. Clearly, the thick debris-layer in *configuration 2* protects the ice from melting compared to *configuration 1* when the same parameter set is employed to bare ice. Conversely, *configuration 3* shows that removal of the debris layer and allows rapid melting and very high mass loss. The area-averaged melt rate in the debris-covered area in *configurations 4* is 85 % lower than *configuration 3*, suggesting the thick debris layer reduces melt rates by this amount.

It is clear from Fig. 8a and 9 that the glacier area changes have a strong influence on mass balance. For example, *configuration 3* shows strongly negative mass balance due to the high relative melt factors and lack of a protective debris surface. However, after 2040, the mass balance tends to be less negative and reaches zero in 2100, due to the removal of the low-lying ablation zone, indicating that the glacier has adapted to the climatic forcing. This is evident in Fig. 9 where very little ice remains below the ice fall. Although *configuration 2* and *3* are not considered realistic scenarios, they reflect the sensitivity of the model to debris cover and provide a means by which we can assess the importance of debris cover to glacier evolution and runoff. The next section will explore this further by employing variable levels of debris.

The Cryosphere Discuss., doi:10.5194/tc-2016-116, 2016
Manuscript under review for journal The Cryosphere
Published: 16 June 2016

4.3.3. Experiment 3: Impact of Ice Cliffs.

Varying the properties of the debris surface, with all other variables remaining constant, significantly affects ice loss and discharge, as demonstrated in Fig. 9 and 10 where *configuration 4A* (thick debris) shows a slower rate of volume loss compared to *configurations 4B, C* and *D* (*4B*: ice cliffs; *4C:* Increased ice cliffs; *4D*: thin debris). Clearly, the protective influence of the debris diminishes with debris disintegration, with the thin debris surface protecting the ice only slightly compared to bare ice. Similarly, Fig. 9e-f demonstrate how the increased proportion of ice-cliff features, in *configuration 4B* compared to 4C, promotes faster loss of ice. These changes are captured in simulated runoff (Fig. 10b) with highest discharge occurring where there is no debris (*configuration 3*) or thin debris (*configuration 4D*) during the period of rapid mass loss (2010-~2070). After 2070, discharge for *configurations 3* and *4D* decreases below the more insulated configurations (*4A, 4B, 4C*) as minimal ice remains beneath the ice-fall (Figure 9c and 9d). Since our knowledge of debris thickness distribution and the impact of ice cliffs are very limited, this sensitivity analysis demonstrates how significantly glacier and runoff evolution are influenced by different debris surfaces.

4.4. Future Evolution of the Khumbu Glacier.

Using the most representative model configuration, this section will provide an estimate of future glacier evolution and runoff. Discharge observations from the Pheriche station from during 2014 are used to provide an indication of which model configuration is most representative of observed conditions. Figure 11 shows monthly and annual discharge from Pheriche in 2014, compared to simulated discharge. Using the Nash-Sutcliffe Efficiency (NSE; Nash & Sutcliffe, 1970) to evaluate performance, discharge is more accurately simulated using *configuration 4A* (thick debris) both annually and daily (NSE = 0.84), compared to *configuration 1* (bare ice; NSE = 0.76). Thus, the debris configuration can be deemed more representative, and is employed for future simulations.

Figure 12 shows the future evolution of glacier retreat and runoff for bias-corrected RCA4 and REMO output. Clearly, ice volume is simulated to decrease for all scenarios until 2100. For RCA4, the remaining ice volume of RCP 2.6 is 40.3 % of initial volume, compared to 28.4 % and 14.5 % for RCP 4.5 and RCP 8.5, respectively. Using REMO output, remaining volume for RCP 4.5 is 25.4 % compared to only 2.6 % for RCP 8.5.

Discharge simulations (Fig. 12b) show minor long-term differences between simulations, with all RCPs showing peak discharge around 2040-55, followed by a net decrease of 8 million m^3 yr^{-1} by 2100 compared to current levels. This initial increase can be explained as additional water production from melting ice, followed by the eventual decrease in discharge once most of this ice reservoir has melted, when snow melt and rainfall will be more significant sources of runoff.

5 Discussion.

5.1. Sensitivity of runoff to debris cover.

5.1.1. Similar volume change in configurations 1 and 4.

The results shown in Fig. 8c (*config. 1*- no consideration of debris; and *config. 4*- debris included) suggest that highly parameterised mass balance models will simulate similar future glacier evolution, regardless of the complexity of debris-cover representation in the model. This occurs because the calibration procedure dictates that the model reproduces observed changes, so the climatic sensitivity of the parameters remains constant over the 21st century, with no significant feedbacks caused by the debris, although a key assumption of this calibration is that debris conditions and climatic sensitivity remain constant in the future. This suggests that future work should focus on enhancing calibration, for example, by increasing the

The Cryosphere Discuss., doi:10.5194/tc-2016-116, 2016
Manuscript under review for journal The Cryosphere
Published: 16 June 2016

number of discharge monitoring stations, and better understanding the temporal changes in debris thickness, rather than increasing model complexity.

However, it would be incorrect to conclude that debris cover is not an important variable, since the results of the sensitivity analysis show considerable uncertainties resulting from incorrectly incorporating debris cover, or when debris cover is not static; a key assumption of *configuration 4* is that debris cover remains constant. For example, the difference between the *bare-ice* parameters and the *debris-cover* parameters in Table 4 reflects the impact debris cover has on glacier melt. This is an example of highly parameterised models yielding the correct results for the wrong reasons. Moreover, the evolution of the debris cover as the glacier changes over time, and the strong feedback with mass balance, will lead to non-linear change. Therefore, it is suggested that efforts are made to improve the understanding and monitoring of temporal changes in the debris surface, so that debris can be realistically incorporated into modelling studies.

5.1.2. Differences in discharge in 'calibrated simulations' (configurations 1 and 4).

The considerable differences in runoff between *configurations 1* (no consideration of debris) and *4* (thick debris; Fig. 8b), despite near-identical volume changes, are likely to be caused by limitations of hydrological models in alpine catchments, whereby processes outside of the glacier influence runoff. Specifically, in the case of clean ice, the low relative melt parameters allow the non-plausible build-up of snow and ice outside of the glacier mask, thus potential water is stored and runoff is reduced. For thick debris, which is a more realistic representation of Khumbu Glacier, the melt parameters are high enough to melt this snow and ice thus generating runoff. This deficiency of hydrological models has been seen in several studies (e.g. Frey and Holzmann, 2015; Bernhardt and Schulz, 2010) but has not received much attention and suggests that snow is accumulating in areas where there is none in reality and that snow redistribution through avalanching may not be realistically captured by the model. This is significant as, during the calibration period, the non-glacial area contributed 70.7 % of total annual runoff.

However, the more accurate reproduction of observed discharge in the debris-covered model *configuration 1* (Fig. 11), suggests that runoff projections only calibrated to glacier changes, without considering the insulating effect of surface debris, may underestimate runoff. Therefore, it is essential that locally calibrated models need to be confident that the ice surface conditions to which they are calibrated will remain constant for the duration of the future simulation. Changes in the nature of the debris surface, for example, disintegration through increased proportion of ice cliffs and melt ponds (Rowan et al., 2015; Benn et al., 2012), remains a considerable area of limited understanding, and their future propagation may alter the climatic sensitivity of the glacier, as shown in Fig. 9-10.

5.2. Debris and Stagnation.

5.2.1. Debris Sensitivity Analysis.

The differences between *configurations 1* to *4* (Fig. 8-9) highlight the impact of debris cover in melt reduction. For example, the reduction in melt rates between thick debris and no debris (*configurations 4* and *3* respectively) of up to 85 % corroborate findings of Ragettli et al. (2015) and suggest that previous studies underestimate reduction factors of melt under debris (Immerzeel et al., 2013; Konz et al., 2007). Although this value is influenced by the choice of debris layer implemented, for example, here the *thick debris* layer of Rowan et al. (2015) is implemented, 85 % represents the maximum reduction of melt, considering uncertainties in the true nature of the debris surface. In terms of ice volume changes, the remaining ice in 2100 ranges from 0.07 km^3 (2.25 % relative to 2010) to 2.17 km^3 (71.7 %). Discharge in 2100 ranges from 57 to 87.5 million m^3 yr^{-1}, depending on the debris scenario, and shows an even larger range in 2010 when the maximum ice volume is available for melt (57-142 million m^3 yr^{-1}).

The Cryosphere Discuss., doi:10.5194/tc-2016-116, 2016
Manuscript under review for journal The Cryosphere
Published: 16 June 2016

Ice cliffs and the properties of the debris surface influence simulated volume change and discharge (Fig. 9 and 10), with increasing debris disintegration promoting mass losses and corresponding increases in discharge. Despite ongoing efforts to simulate ice-cliff and melt-pond processes (e.g. Miles et al., 2016; Steiner et al., 2015; Sakai et al., 2000), the understanding regarding their future evolution in terms of their number, size and distribution, is limited. In particular, the impact of ice cliffs and melt ponds at glacier scale and how to implement these key features into models is largely unknown. Although ice-cliff and melt-pond features have been incorporated into this study through a sensitivity experiment using locally enhanced melt rates, the current level of understanding of ice-cliff and melt-pond evolution and dynamics is too limited to realistically simulate their impact and evolution.

5.2.2. Debris expansion and thickening.

Although it is possible to implement spatially expanding debris by using a scheme similar to that of Jouvet et al. (2011), this is not necessary at Khumbu because the spatial extent of debris is unlikely to change significantly before 2100 due to the current ELA (Equilibrium Line Altitude) elevation of around 5600 m (Bolch et al., 2011; Benn and Lehmkuhl, 2000). This falls mid-way up the Khumbu ice-fall acting as a divide above which there is very little debris due to the high accumulation and low ablation at high elevations. Rowan et al. (2015) explores the evolution of debris on Khumbu and simulates minimal debris above the ice-fall, even in 2200. However, this situation is specific to Khumbu Glacier, therefore, it is desirable to incorporate spatially evolving debris into models at other sites, either using a relatively simple scheme, such as Jouvet et al. (2011), or using a dynamic debris-evolution model, such as in Rowan et al. (2015).

Debris thickness is expected to thicken with continued stagnation and downwasting (Hambrey et al., 2009). To test the impact a thickening debris cover will have on melt, *configuration 4* simulations were repeated using only RCP 4.5 from RCA4, only with a debris thickening scheme whereby debris thickness continually thickens until 2100, realised by continually decreasing the debris reduction factor (f_{debris}) to mimic a thickening of 50 cm by 2100. The results of this experiment show less than 1 % decrease in simulated volume change and mean discharge, suggesting the thickening debris will have a negligible impact since the majority of debris on Khumbu Glacier is already thick enough to significantly reduce melt.

5.2.3. Testing different Δh curves of mass redistribution.

The Δh-approach to mass redistribution uses a calibrated redistribution curve (Fig. 2) based on the geodetic survey of Nuimura et al. (2012). By repeating future simulations with a non-calibrated curve which assumes mass loss through frontal recession, it is possible to investigate how applicable 'typical' retreat assumptions are to debris-covered glaciers. Using the non-calibrated curve, the spatial ice loss is more typical of non-debris-covered glaciers, showing clear terminus recession, whereas the Khumbu-specific curve reduces terminus recession but incorporates the mass loss through downwasting (Fig. S5). Thus, it is recommended that correctly capturing the pattern of mass loss, for example using geodetic data or dynamic glacier modelling, is prioritised in future modelling studies.

5.3. The Future Evolution of Khumbu Glacier.

The most 'representative' model configuration and the suite of climate scenarios simulated significant ice volume losses in the 21st century (Fig. 12). Although the range of scenarios reflects considerable uncertainty in the climate signals, there is broad agreement that remaining ice volume will be significantly reduced. In 2100, the simulated ice volume ranges from 2.6 % of 2010 volume for REMO-RCP 8.5, to 40 % of 2010 volume for RCA4-RCP 2.6. The pattern of continued ice loss agrees with simulations of other studies. For example, Shea et al. (2015) estimated remaining ice volumes of 4 to 27% in

The Cryosphere Discuss., doi:10.5194/tc-2016-116, 2016
Manuscript under review for journal The Cryosphere
Published: 16 June 2016

2100 for all glaciers in the Everest region and Immerzeel et al. (2013; 2012) simulates continued volume losses during the 21st century at the Langtang catchment. The manifestation of this mass loss is through a combination of thinning and terminus recession at low elevations, whereas high elevations remain relatively unchanged (Fig. 9). This high elevation accumulation zone may contain a greater or lesser volume of ice than this study simulates, as there are understandably no observations of ice thickness available. Moreover, the simulated mass loss at low elevations reflects a loss of active ice that is no longer sustainably replenished in mass from higher elevations; however, it is likely that a large amount of *dead ice* will remain beneath thick debris layers (Benn et al., 2012; Humlum, 1998). This dead ice, which is not included in future ice volume, may explain the significant differences in glacier evolution simulated in this study and in Rowan et al., (2015) who show limited ice thinning in the debris-covered areas of Khumbu Glacier in the future. However, both studies agree that the debris-covered tongue is likely to detach from the upper glacier in the future as the currently active ice area retreats further up-glacier.

The simulated peak discharge in 2040-2055 followed by an eventual decrease (Fig. 12) agree with Rees and Collins, (2006) and Immerzeel et al. (2010), who simulate catchment runoff at different scales. However, Immerzeel et al. (2013) found increasing trends in river flows for the Baltoro and Langtang Glaciers, relative to 1961-1990. The main factors explaining the differing trends between studies are the differing precipitation trends and the scale of the study area.

5.4. Overall uncertainty Analysis.

The lack of long-term meteorological, hydrological and glaciological data makes it difficult to estimate the uncertainty associated with the simulations, since the model performance cannot be extensively validated against past changes in glacier evolution and catchment runoff. The performance of simulated runoff compared to the short runoff observations are encouraging (Fig. 11), but it should be emphasised that the future simulations in this study are highly uncertain. The focus of this study is to better understand the uncertainties associated with debris cover in terms of glacier and runoff evolution; however a brief summary of other sources of uncertainty is discussed. Huss et al. (2014) provides a thorough review of uncertainties associated with glacio-hydrological modelling.

Firstly, the estimates of future climate change are limited by the performance of GCM and RCM simulations over extreme topography (e.g. Kotlarski et al., 2014; Prömmel et al., 2010). Although every care has been taken to include a comprehensive bias-correction process, the lack of observations, particularly regarding precipitation, at high altitude hampers understanding of climatology in the Himalaya. Subsequently, the reanalysis datasets used to drive evaluation simulations and used in the bias correction process, are constrained by limited observations so are unlikely to be as accurate as those in more accessible mountain regions with longer records, for example, the European Alps. Recent decreasing trends in precipitation in the Everest region (Salerno et al., 2015) are only captured by two out of five simulations, although it is not possible to know whether this trend is a result of external forcing, or is due to internal climate variability, and whether it will continue. Only the RCA4 and REMO RCM simulations were available at the time of writing, which limits the constraint of RCM uncertainty. Moreover, the limited uptake of CORDEX-South Asia simulations in published literature to date results in a lack of understanding of the relative performance of these RCMs in extreme topography. Therefore, it is urged that a study similar to that of Kotlarski et al. (2014), who evaluated the performance of CORDEX-Europe simulations over the Alps, is conducted in other CORDEX domains.

There are considerable uncertainties associated with the calibration of GERM to geodetic mass balance. Firstly, the geodetic mass balance surveys contain uncertainty associated with stereographically deriving DEMs in steep terrain (Nuimura et al., 2012; Bolch et al., 2011) and low contrast in high-elevation accumulation areas, for example. For this study, the geodetic mass balance of -0.51 m w.e. yr^{-1} from Gardelle et al. (2013) is associated with an uncertainty of ± 0.19 m w.e.

The Cryosphere Discuss., doi:10.5194/tc-2016-116, 2016
Manuscript under review for journal The Cryosphere
Published: 16 June 2016

yr^{-1}. Moreover, Figure 7 shows that geodetic mass balance estimates do vary between different studies, further corroborated by Bolch et al. (2011) who provide an additional geodetic survey of Khumbu Glacier from 1970-2007, finding a specific mass balance of -0.27 m w.e. yr^{-1}. This variability makes validation of the model problematic; however, the broad agreement and the widespread trend in the Himalayan region suggests that current trends are indicative of a longer term climate response.

The lack of multiple calibration data sets, for example, volume change and snow accumulation, create problems in terms of the cause of volume changes. For example, correct volume loss can be attained through incorrect simulation of accumulation and ablation since volume change alone does not indicate the source of runoff (Pellicciotti et al., 2012; Schaefli and Huss, 2011; Konz and Seibert, 2010). In this study, the simulated discharge agrees relatively well with short-term discharge observations at Pheriche (Fig. 11), reaffirming that volume losses are being calculated reasonably well. Finally, the stationarity of model parameters is a known limitation of highly-calibrated models, assuming that the current relationship between climate and snow and ice melt will remain constant until 2100 (Huss et al., 2008a).

Uncertainties associated with the delineation of the glacier mask are significant due to difficulties discerning between ice, debris-covered ice, snow, and rock (Paul et al. 2013), which is further complicated by the abundance of stagnant and dead ice, the classification of which is not straightforward. The Randolph Glacier Inventory used in this study is standardised and checked for errors and allows comparison of different catchments in different regions (Pfeffer et al., 2014). However, Vincent et al. (2016) used repeat differential-GPS measurements to determine glacier flow on Changri Nup Glacier and found the extent of the active ice to be considerably smaller than the Randolph Inventory suggests. Such a difference raises the possibility that the inventory may overestimate glacier area in other areas which would influence ice volume estimates as well as future runoff simulation. Therefore, it is suggested that a detailed evaluation of glacier inventory data in the Himalayas is conducted with an emphasis on assessing the delineation of active and stagnant ice.

6 Conclusions.

This study has investigated the relationship between debris cover and glacier and runoff evolution at Khumbu Glacier by modifying a temperature-index model to incorporate fully distributed debris cover. The results of calibrated model simulations indicate that future simulations of glacier evolution are not strongly influenced by explicit incorporation of debris, assuming that the climate sensitivity and debris conditions remain constant during the simulation.

However, since the future evolution of debris is not fully understood, a sensitivity analysis was performed to assess the sensitivity of model outputs to changing debris cover. The large range of volume change estimates between configurations represents the maximum errors possible for debris cover changes, and highlights the insulating influence of debris cover. Moreover, due to the large uncertainties concerning the thickness of debris and the lack of understanding of the impacts of ice cliffs and melt ponds, a variety of debris surfaces with varying degrees of ice-cliff coverage are included, indicating that increased debris defragmentation enhances melt and volume losses.

Finally, simulations of glacier and runoff evolution are performed using two bias-corrected RCMs to simulate the future evolution of the Khumbu Glacier. These simulations indicate that remaining ice volume in 2100 will be between 2.6 % and 40 % of volume in 2010, depending on climate model and scenario, with the loss of much of the lower elevation ice in all scenarios. Discharge is expected to peak from 2040-2055 and reduce compared to 2010 levels by ~8 % by 2100. However, there remain significant uncertainties associated with many elements of the simulations, so the results of these simulations should be treated with caution. Specifically, the limited observations and understanding of precipitation at high elevations in the Himalayas, together with the limitations of GCMs and RCMs to accurately reproduce precipitation, introduce significant

uncertainties. Moreover, the limited understanding of debris-covered surfaces will evolve, including how changes to ice cliffs and supra-glacial ponds will impact ablation, introduce the most significant uncertainties.

Acknowledgements. This study was funded by the EPSRC (Research Council UK). We acknowledge the World Climate Research Programme for coordinating CORDEX-South Asia and the Swedish Meteorological and Hydrological Institute (SMHI) and Climate Service Centre Germany (GERICS) climate modelling groups for making data available. Location of melt ponds were provided by Cameron Watson. Debris surfaces were provided by David Rounce and Ann Rowan. The bias-correction approach was significantly improved thanks to advice from Martin Widmann, Ernesto Pastén Zapata and Nicolas Guyennon. Ann Rowan provided advice on the modelling experiments and commented on an earlier draft. This work was supported by the MIUR through Ev-K2-CNR/SHARE and CNR-DTA/NEXTDATA project within the framework of the Ev-K2-CNR and Nepal Academy of Science and Technology (NAST). Daniele Bocchiola is thanked for the stage-discharge curve.

References.

Ageta, Y., Fujita, K.: Characteristics of mass balance of summeraccumulation type glaciers in the Himalayas and Tibetan Plateau, Gletscherkd, Glazialgeol, 32(61-65), 1996.

Akhtar, M., Ahmad, N. and Booij, M. J.: The impact of climate change on the water resources of Hindukush–Karakorum–Himalaya region under different glacier coverage scenarios, J. Hydrol., 355(1-4), 148–163, doi:10.1016/j.jhydrol.2008.03.015, 2008.

Anderson, R. S.: A model of ablation-dominated medial moraines and the generation of debris-mantled glacier snouts, J. Glaciol., 46(154), 459–469 , 2000.

Benn, D. I. and Lehmkuhl, F.: Mass balance and equilibrium-line altitudes of glaciers in high-mountain environments, Quat. Int., 65-66, 15–29, doi:10.1016/S1040-6182(99)00034-8, 2000.

Benn, D. I., Bolch, T., Hands, K., Gulley, J., Luckman, A., Nicholson, L. I., Quincey, D., Thompson, S., Toumi, R. and Wiseman, S.: Response of debris-covered glaciers in the Mount Everest region to recent warming, and implications for outburst flood hazards, Earth-Science Rev., 114(1-2), 156–174, doi:10.1016/j.earscirev.2012.03.008, 2012.

Bernhardt, M. and Schulz, K.: SnowSlide: A simple routine for calculating gravitational snow transport, Geophys. Res. Lett., 37(11), 1–6, doi:10.1029/2010GL043086, 2010.

Bolch, T., Buchroithner, M. F., Peters, J., Baessler, M. and Bajracharya, S.: Identification of glacier motion and potentially dangerous glacial lakes in the Mt. Everest region/Nepal using spaceborne imagery, Nat. Hazards Earth Syst. Sci., 8(6), 1329–1340, doi:10.5194/nhess-8-1329-2008, 2008.Bolch, T., Pieczonka, T. and Benn, D. I.: Multi-decadal mass loss of glaciers in the Everest area (Nepal Himalaya) derived from stereo imagery, Cryosph., 5(2), 349–358, doi:10.5194/tc-5-349-2011, 2011.

Collier, E., Maussion, F., Nicholson, L. I., Mölg, T., Immerzeel, W. W. and Bush, A. B. G.: Impact of debris cover on glacier ablation and atmosphere–glacier feedbacks in the Karakoram, Cryosph., 9(4), 1617–1632, doi:10.5194/tc-9-1617-2015, 2015.

Cuffey, K. M. and Paterson, W. S. . B.: Physics of Glaciers, Fourth Edition, Academic Press, 2010.

Farinotti, D., Usselmann, S., Huss, M., Bauder, A. and Funk, M.: Runoff evolution in the Swiss Alps: projections for selected high-alpine catchments based on ENSEMBLES scenarios, Hydrol. Process., 26(13), 1909–1924, doi:10.1002/hyp.8276, 2012.

Frey, S. and Holzmann, H.: A conceptual, distributed snow redistribution model, Hydrol. Earth Syst. Sci., 19(11), 4517–4530, doi:10.5194/hess-19-4517-2015, 2015.

Fujita, K. and Sakai, A.: Modelling runoff from a Himalayan debris-covered glacier, Hydrol. Earth Syst. Sci., 18(7), 2679–2694, doi:10.5194/hess-18-2679-2014, 2014.

Fyffe, C. L., Reid, T. D., Brock, B. W., Kirkbride, M. P., Diolaiuti, G., Smiraglia, C. and Diotri, F.: A distributed energy-balance melt model of an alpine debris-covered glacier, J. Glaciol., 60(221), 587–602, doi:10.3189/2014JoG13J148, 2014.

Gades, A., Conway, H., Nereson, N., Naito, N. and Kadota, T.: Radio echo-sounding through supraglacial debris on Lirung and Khumbu Glaciers, Nepal Himalayas, IAHS Publ., 264(264), 13–22, 2000.

Glen, J. W., The creep of polycrystalline ice, Proc. R. Soc. London, 228(1175), 519-538, 1955.

Gardelle, J., Berthier, E., Arnaud, Y. and Kääb, A.: Region-wide glacier mass balances over the Pamir-Karakoram-Himalaya during 1999–2011, Cryosph., 7(4), 1263–1286, doi:10.5194/tc-7-1263-2013, 2013.

Hambrey, M. J., Quincey, D. J., Glasser, N. F., Reynolds, J. M., Richardson, S. J. and Clemmens, S.: Sedimentological, geomorphological and dynamic context of debris-mantled glaciers, Mount Everest (Sagarmatha) region, Nepal, Quat. Sci. Rev., 28(25-26), 1084, doi:10.1016/j.quascirev.2009.04.009, 2009.

Hock, R.: A distributed temperature-index ice-and snowmelt model including potential direct solar radiation, J. Glaciol.,

45(149), 101–111, 1999.
Humlum, O.: The climatic significance of rock glaciers, Permafr. Periglac. Process., 9(4), 375–395, doi:10.1002/(SICI)1099-1530(199810/12)9:4<375::AID-PPP301>3.0.CO;2-0, 1998.
Huss, M. and Farinotti, D.: Distributed ice thickness and volume of all glaciers around the globe, J. Geophys. Res., 117(F4), F04010, doi:10.1029/2012JF002523, 2012.
Huss, M. and Hock, R.: A new model for global glacier change and sea-level rise, Front. Earth Sci., 3, 1–22, doi:10.3389/feart.2015.00054, 2015.
Huss, M., Bauder, A., Funk, M. and Hock, R.: Determination of the seasonal mass balance of four Alpine glaciers since 1865, J. Geophys. Res., 113(F1), F01015, doi:10.1029/2007JF000803, 2008a.
Huss, M., Farinotti, D., Bauder, A. and Funk, M.: Modelling runoff from highly glacierized alpine drainage basins in a changing climate, Hydrol. Process., 22(19), 3888–3902, doi:10.1002/hyp.7055, 2008b.
Huss, M., Jouvet, G., Farinotti, D. and Bauder, A.: Future high-mountain hydrology: a new parameterization of glacier retreat, Hydrol. Earth Syst. Sci., 14(5), 815–829, doi:10.5194/hess-14-815-2010, 2010.
Huss, M., Zemp, M., Joerg, P. C. and Salzmann, N.: High uncertainty in 21st century runoff projections from glacierized basins, J. Hydrol., 510, 35–48, doi:10.1016/j.jhydrol.2013.12.017, 2014.
Ichiyanagi, K., Yamanaka, M. D., Muraji, Y. and Vaidya, B. K.: Precipitation in Nepal between 1987 and 1996, Int. J. Climatol., 27(13), 1753–1762, doi:10.1002/joc.1492, 2007.
Immerzeel, W. W., van Beek, L. P. H. and Bierkens, M. F. P.: Climate Change Will Affect the Asian Water Towers, Science 328(5984), 1382–1385, doi:10.1126/science.1183188, 2010.
Immerzeel, W. W., van Beek, L. P. H., Konz, M., Shrestha, A. B. and Bierkens, M. F. P.: Hydrological response to climate change in a glacierized catchment in the Himalayas., Clim. Change, 110(3-4), 721–736, doi:10.1007/s10584-011-0143-4, 2012.
Immerzeel, W. W., Pellicciotti, F. and Bierkens, M. F. P.: Rising river flows throughout the twenty-first century in two Himalayan glacierized watersheds, Nat. Geosci., 6(9), 742–745, doi:10.1038/ngeo1896, 2013.
Inoue, J.: Mass budget of Khumbu Glacier, Seppyo1, 39, 15–19, 1977.
Inoue, J. and Yoshida, M.: Ablation and Heat Exchange over the Khumbu Glacier, J. Japanese Soc. Snow Ice, 41(Special), 26–33, doi:10.5331/seppyo.41.Special_26, 1980.
Jacob, D.: Regional Climate Models: Linking Global Climate Change to Local Impacts, in Encyclopedia of Complexity and Systems Science, edited by A. R. Meyers, pp. 7591–7602, Springer New York, New York, NY., 2009.
Jacob, D. and Podzun, R.: Sensitivity studies with the regional climate model REMO, Meteorol. Atmos. Phys., 63(1-2), 119–129, 1997.
Jost, G., Moore, R. D., Menounos, B. and Wheate, R.: Quantifying the contribution of glacier runoff to streamflow in the upper Columbia River Basin, Canada, Hydrol. Earth Syst. Sci., 16(3), 849–860, doi:10.5194/hess-16-849-2012, 2012.
Jouvet, G., Huss, M., Funk, M. and Blatter, H.: Modelling the retreat of {G}rosser {A}letschgletscher, {S}witzerland, in a changing climate, J. Glaciol., 57(206), 1033–1045, doi:10.3189/002214311798843359, 2011.
Kaab, A., Berthier, E., Nuch, C., Gardelle, J., and Arnaud, Y., Contrasting patterns of early twenty-first-century glacier mass change in the Himalayas, Nature 488(7412): 495-498, 2012.
Kehrwald, N. M., Thompson, L. G., Tandong, Y., Mosley-Thompson, E., Schotterer, U., Alfimov, V., Beer, J., Eikenberg, J. and Davis, M. E.: Mass loss on Himalayan glacier endangers water resources, Geophys. Res. Lett., 35(22), L22503, doi:10.1029/2008GL035556, 2008.
Konz, M. and Seibert, J.: On the value of glacier mass balances for hydrological model calibration, J. Hydrol., 385(1-4), 238–246, doi:10.1016/j.jhydrol.2010.02.025, 2010.
Konz, M., Uhlenbrook, S., Braun, L., Shrestha, A. and Demuth, S.: Implementation of a process-based catchment model in a poorly gauged, highly glacierized Himalayan headwater, Hydrol. Earth Syst. Sci., 11(4), 1323–1339, 2007.
Kotlarski, S., Keuler, K., Christensen, O. B., Colette, A., Déqué, M., Gobiet, A., Goergen, K., Jacob, D., Lüthi, D., van Meijgaard, E., Nikulin, G., Schär, C., Teichmann, C., Vautard, R., Warrach-Sagi, K. and Wulfmeyer, V.: Regional climate modeling on European scales: a joint standard evaluation of the EURO-CORDEX RCM ensemble, Geosci. Model Dev., 7(4), 1297–1333, doi:10.5194/gmd-7-1297-2014, 2014.
Li, H., Beldring, S., Xu, C., Huss, M., Melvold, K. and Jain, S. K.: Integrating a glacier retreat model into a hydrological model – Case studies of three glacierised catchments in Norway and Himalayan region, 527, 656–667, doi:10.1016/j.jhydrol.2015.05.017, 2015.
Miles, E. S., Pellicciotti, F., Willis, I. C., Steiner, J. F., Buri, P. and Arnold, N. S.: Refined energy-balance modelling of a supraglacial pond, Langtang Khola, Nepal, Ann. Glaciol., 57(71), 29–40, doi:10.3189/2016AoG71A421, 2016.
Miller, J. D., Immerzeel, W. W. and Rees, G.: Climate Change Impacts on Glacier Hydrology and River Discharge in the Hindu Kush–Himalayas, Mt. Res. Dev., 32(4), 461–467, doi:10.1659/MRD-JOURNAL-D-12-00027.1, 2012.
Moribayashi, S.: Transverse profiles of Khumbu Glacier obtained by gravity observation: glaciological expedition of Nepal., Seppyo, 46(40), 21–25, 1978.
Nash, J. E. and Sutcliffe, J. V.: River flow forecasting through conceptual models part I — A discussion of principles, J. Hydrol., 10(3), 282–290, doi:10.1016/0022-1694(70)90255-6, 1970.
Nicholson, L. and Benn, D. I.: Calculating ice melt beneath a debris layer using meteorological data, J. Glaciol., 52(178), 463–470, doi:10.3189/172756506781828584, 2006.

Nicholson, L. and Benn, D. I.: Properties of natural supraglacial debris in relation to modelling sub-debris ice ablation, Earth Surf. Process. Landforms, 38(5), 490–501, doi:10.1002/esp.3299, 2013.

Nuimura, T., Fujita, K., Yamaguchi, S. and Sharma, R. R.: Elevation changes of glaciers revealed by multitemporal digital elevation models calibrated by GPS survey in the Khumbu region, Nepal Himalaya, 1992–2008, J. Glaciol., 58(210), 648–656, doi:10.3189/2012JoG11J061, 2012.

Østrem, G. Ice melting under a thin layer of moraine, and the existence of ice cores in moraine ridges. Geogr. Ann.41, 228–230. 1959.

Pellicciotti, F., Buergi, C., Immerzeel, W. W., Konz, M. and Shrestha, A. B.: Challenges and Uncertainties in Hydrological Modeling of Remote Hindu Kush–Karakoram–Himalayan (HKH) Basins: Suggestions for Calibration Strategies, Mt. Res. Dev., 32(1), 39–50, doi:10.1659/MRD-JOURNAL-D-11-00092.1, 2012.

Pfeffer, W. T., Arendt, A. A., Bliss, A., Bolch, T., Cogley, J. G., Gardner, A. S., Hagen, J.-O., Hock, R., Kaser, G., Kienholz, C., Miles, E. S., Moholdt, G., Mölg, N., Paul, F., Radić, V., Rastner, P., Raup, B. H., Rich, J. and Sharp, M. J.: The Randolph Glacier Inventory: a globally complete inventory of glaciers, J. Glaciol., 60(221), 537–552, doi:10.3189/2014JoG13J176, 2014.

Piani, C., Haerter, J. O. and Coppola, E.: Statistical bias correction for daily precipitation in regional climate models over Europe, Theor. Appl. Climatol., 99(1-2), 187–192, doi:10.1007/s00704-009-0134-9, 2010.

Pratap, B., Dobhal, D. P., Mehta, M. and Bhambri, R.: Influence of debris cover and altitude on glacier surface melting: a case study on Dokriani Glacier, central Himalaya, India, Ann. Glaciol., 56(70), 9–16, doi:10.3189/2015AoG70A971, 2015.

Prömmel, K., Geyer, B., Jones, J. M. and Widmann, M.: Evaluation of the skill and added value of a reanalysis-driven regional simulation for Alpine temperature, Int. J. Climatol., 30(5), 760–773, doi:10.1002/joc.1916, 2010.

Quincey, D. J., Luckman, A. J. and Benn, D. I.: Quantification of Everest region glacier velocities between 1992 and 2002, using satellite radar interferometry and feature tracking, J. Glaciol., 55(192), 596–606, doi:10.3189/002214309789470987, 2009.

Ragettli, S., Pellicciotti, F., Immerzeel, W. W., Miles, E. S., Petersen, L., Heynen, M., Shea, J. M., Stumm, D., Joshi, S. and Shrestha, A.: Unraveling the hydrology of a Himalayan catchment through integration of high resolution in situ data and remote sensing with an advanced simulation model, Adv. Water Resour., 78, 94–111, doi:10.1016/j.advwatres.2015.01.013, 2015.

Rees, H. G. and Collins, D. N.: Regional differences in response of flow in glacier-fed Himalayan rivers to climatic warming, in Hydrological Processes, vol. 20, pp. 2157–2169., 2006.

Reid, T. D. and Brock, B. W.: Assessing ice-cliff backwasting and its contribution to total ablation of debris-covered Miage glacier, Mont Blanc massif, Italy, J. Glaciol., 60(219), 3–13, doi:10.3189/2014JoG13J045, 2014.

Rounce, D. R. and McKinney, D. C.: Debris thickness of glaciers in the Everest area (Nepal Himalaya) derived from satellite imagery using a nonlinear energy balance model, Cryosph., 8(4), 1317–1329, doi:10.5194/tc-8-1317-2014, 2014.

Rounce, D. R., Quincey, D. J. and McKinney, D. C.: Debris-covered glacier energy balance model for Imja–Lhotse Shar Glacier in the Everest region of Nepal, Cryosph., 9(6), 2295–2310, doi:10.5194/tc-9-2295-2015, 2015.

Rowan, A. V, Egholm, D. L., Quincey, D. J. and Glasser, N. F.: Modelling the feedbacks between mass balance, ice flow and debris transport to predict the response to climate change of debris-covered glaciers in the Himalaya, Earth Planet. Sci. Lett., 430, 427–438, doi:10.1016/j.epsl.2015.09.004, 2015.

Sakai, A., Nakawo, M. and Fujita, K.: Melt rate of ice cliffs on the Lirung Glacier, Nepal Himalayas, 1996, Bull. Glacier Res., 16(October), 57–66, 1998.

Sakai, A., Takeuchi, N., Fujita, K. and Nakawo, M.: Role of supraglacial ponds in the ablation process of a debris-covered glacier in the Nepal Himalayas, IAHS Publ., (265), 119–130, 2000.

Salerno, F., Guyennon, N., Thakuri, S., Viviano, G., Romano, E., Vuillermoz, E., Cristofanelli, P., Stocchi, P., Agrillo, G., Ma, Y. and Tartari, G.: Weak precipitation, warm winters and springs impact glaciers of south slopes of Mt. Everest (central Himalaya) in the last 2 decades (1994–2013), Cryosph., 9(3), 1229–1247, doi:10.5194/tc-9-1229-2015, 2015.

Samuelsson, P., Jones, C. G., Willén, U., Ullerstig, A., Gollvik, S., Hansson, U., Jansson, C., Kjellström, E., Nikulin, G. and Wyser, K.: The Rossby Centre Regional Climate model RCA3: model description and performance, Tellus A, 63(1), 4–23, doi:10.1111/j.1600-0870.2010.00478.x, 2011.

Schaefli, B. and Huss, M.: Integrating point glacier mass balance observations into hydrologic model identification, Hydrol. Earth Syst. Sci., 15(4), 1227–1241, doi:10.5194/hess-15-1227-2011, 2011.

Scherler, D., Bookhagen, B. and Strecker, M. R.: Spatially variable response of Himalayan glaciers to climate change affected by debris cover, Nat. Geosci., 4(3), 156–159, doi:10.1038/ngeo1068, 2011.

Sharma, D., Gupta, A. Das and Babel, M. S.: Spatial disaggregation of bias-corrected GCM precipitation for improved hydrologic simulation: Ping River Basin, Thailand, Hydrol. Earth Syst. Sci., 11(4), 1373–1390, 2007.

Shea, J. M., Immerzeel, W. W., Wagnon, P., Vincent, C. and Bajracharya, S.: Modelling glacier change in the Everest region, Nepal Himalaya, Cryosph., 9(3), 1105–1128, doi:10.5194/tc-9-1105-2015, 2015.

Sorg, A., Huss, M., Rohrer, M. and Stoffel, M.: The days of plenty might soon be over in glacierized Central Asian catchments, Environ. Res. Lett., 9(10), 104018, doi:10.1088/1748-9326/9/10/104018, 2014.

Steiner, J. F., Pellicciotti, F., Buri, P., Miles, E. S., Immerzeel, W. W. and Reid, T. D.: Modelling ice-cliff backwasting on a debris-covered glacier in the Nepalese Himalaya, J. Glaciol., 61(229), 889–907, doi:10.3189/2015JoG14J194, 2015.

Taylor, K. E., Stouffer, R. J. and Meehl, G. a: A Summary of the CMIP5 Experiment Design, World, 4(January 2011), 1–33, doi:10.1175/BAMS-D-11-00094.1, 2007.

Thakuri, S., Salerno, F., Smiraglia, C., Bolch, T., D'Agata, C., Viviano, G. and Tartari, G.: Tracing glacier changes since the 1960s on the south slope of Mt. Everest (central Southern Himalaya) using optical satellite imagery, Cryosph., 8(4), 1297–1315, doi:10.5194/tc-8-1297-2014, 2014.

Thakuri, S., Salerno, F., Bolch, T., Guyennon, N. and Tartari, G.: Factors controlling the accelerated expansion of Imja Lake, Mount Everest region, Nepal, Ann. Glaciol., 57(71), 245–257, doi:10.3189/2016AoG71A063, 2015.

Thayyen, R. J., Gergan, J. T. and Dobhal, D. P.: Role of glaciers and snow cover on headwater river hydrology in monsoon regime - Micro-scale study of Din Gad catchment, Garhwal Himalaya, India, Curr. Sci., 92(3), 376–382, 2007.

van Vuuren, D. P., Edmonds, J., Kainuma, M., Riahi, K., Thomson, A., Hibbard, K., Hurtt, G. C., Kram, T., Krey, V., Lamarque, J. F., Masui, T., Meinshausen, M., Nakicenovic, N., Smith, S. J. and Rose, S. K.: The representative concentration pathways: An overview, Clim. Change, 109(1), 5–31, doi:10.1007/s10584-011-0148-z, 2011.

Vincent, C., Wagnon, P., Shea, J. M., Immerzel, W. W., Kraaijenbrink, P. D. A., Shrestha, D., Soruco, A., Arnaud, Y., Brun, F., Berthier, E., and Sherpa, S. F.: Reduced melt on debris-covered glaciers: investigations from Changri Nup Glacier, Nepal, The Cryosphere Discuss., doi:10.5194/tc-2016-75, in review, 2016.

Watson, C. S., Quincey, D. J., Carrivick, J. L. and Smith, M. W.: The dynamics of supraglacial ponds in the Everest region, central Himalaya, Glob. Planet. Change, n.d.

Worni, R., Huggel, C. and Stoffel, M.: Glacial lakes in the Indian Himalayas--from an area-wide glacial lake inventory to on-site and modeling based risk assessment of critical glacial lakes., Sci. Total Environ., 468-469 Su, S71–84, doi:10.1016/j.scitotenv.2012.11.043, 2013.

Xu, J., Grumbine, R. E., Shrestha, A., Eriksson, M., Yang, X., Wang, Y. and Wilkes, A.: The melting Himalayas: cascading effects of climate change on water, biodiversity, and livelihoods., Conserv. Biol., 23(3), 520–30, doi:10.1111/j.1523-1739.2009.01237.x, 2009.

Yang, D. Q., Goodison, B. E., Ishida, S. and Benson, C. S.: Adjustment of daily precipitation data at 10 climate stations in Alaska: Application of World Meteorological Organization intercomparison results, Water Resour. Res., 34(2), 241–256, doi:10.1029/97WR02681, 1998.

Zhang, Y., Fujita, K., Liu, S., Liu, Q. and Nuimura, T.: Distribution of debris thickness and its effect on ice melt at Hailuogou glacier, southeastern Tibetan Plateau, using in situ surveys and ASTER imagery, J. Glaciol., 57(206), 1147–1157, doi:10.3189/002214311798843331, 2011.

The Cryosphere Discuss., doi:10.5194/tc-2016-116, 2016
Manuscript under review for journal The Cryosphere
Published: 16 June 2016

Table 1: Data availability at Khumbu.

Data type	Years	Site/Details	Source	Mass balance (m w.e. yr^{-1})
Meteorological	1994-2013	Pyramid	Salerno et al., 2015	-
Geodetic MB	1999-2010	Khumbu Glacier	Gardelle et al., 2013	-0.51 ± 0.19
	2002-2007	Khumbu Glacier	Bolch et al., 2011	-0.45 ± 0.52
	2000-2008	Khumbu Glacier	Nuimura et al., 2012	-0.76 ± 0.52
	2003-2008	Everest region	Kaab et al., 2012	-0.39 ± 0.11
Discharge	2012-2014	Pheriche	This study	-
Climate – evaluation (ERA-I)	1989-2008	-	CORDEX-South Asia	-
Climate – future (GCM)	2010-2100	-	CORDEX-South Asia	-
Debris Thickness	2002-2008	Remote-sensing	Rounce & McKinney, 2014	-
	2000	Modelled debris	Rowan et al., 2015	-

The Cryosphere Discuss., doi:10.5194/tc-2016-116, 2016
Manuscript under review for journal The Cryosphere
Published: 16 June 2016

Table 2: Range of debris-surfaces, with the configuration(s) in which they are implemented.

Debris Surface	Config.	Source
Bare Ice	1	DEM
Thick Debris	2 & 4A	Rowan et al., 2015
Thick debris + ice cliffs	4B	Rowan et al., 2015 (modified)
Thick debris + increased ice cliffs	4C	Rowan et al., 2015 (modified)
Thin Debris	4D	Rounce & McKinney, 2014

The Cryosphere Discuss., doi:10.5194/tc-2016-116, 2016
Manuscript under review for journal The Cryosphere
Published: 16 June 2016

Table 3: Metrics describing performance of raw RCM "Sim", and the bias-correction "BC", in comparison to observed temperature (TAS) and precipitation (Pr). These metrics are calculated using the independent cross-validation bias correction. Also included are the number of dry days per year and the onset of the melt season, defined as the first period of consecutive warm days (T>0°) lasting more than five days.

RMSE	Pr (mm)	Sim	8.9
		BC	0.8
	TAS (°C)	Sim	5.1
		BC	1.0
Absolute Error	Pr (mm)	Sim	9.3
		BC	0.4
	TAS (°C)	Sim	-9.1
		BC	0.0
Number of Dry days per year	1994-2002	Obs	165
		Sim	143
		BC	197
	2002-2010	Obs	219
		Sim	133
		BC	197
Start of melt season (day of year)	1994-2002	Obs	138
		Sim	171
		BC	135
	2002-2010	Obs	138
		Sim	166
		BC	134

The Cryosphere Discuss., doi:10.5194/tc-2016-116, 2016
Manuscript under review for journal The Cryosphere
Published: 16 June 2016

Table 4: Calibrated parameter sets for the model configurations. *dP/dz* is the precipitation lapse rate; *dT/dz* is the temperature lapse rate. Since precipitation was corrected outside of the modelling process, accumulation parameters are not included in the calibration process.

Parameter	Units	Surface	
		"Bare Ice"	"Thick Debris"
f_M	10^{-3} m (d °C)$^{-1}$	1.104	2.808
r_{ice}	10^{-5} m^3 (W d °C)$^{-1}$	1.752	4.493
r_{snow}	10^{-5} m^3 (W d °C)$^{-1}$	1.104	2.808
dP/dz	10^{-2} % m^{-1}	0	0
dT/dz	10^{-3} °C m^{-1}	-6	-6

The Cryosphere Discuss., doi:10.5194/tc-2016-116, 2016
Manuscript under review for journal The Cryosphere
Published: 16 June 2016

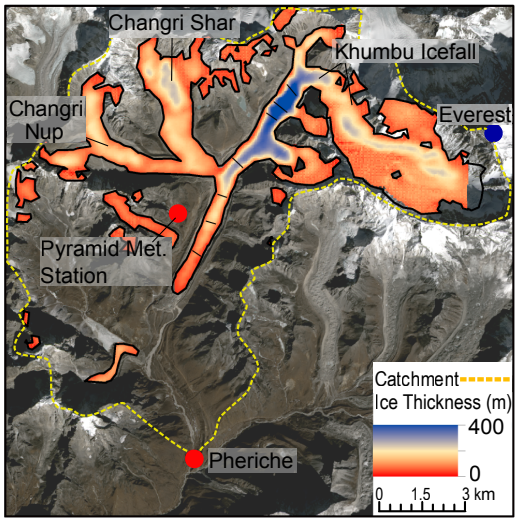

Figure 1: Location of the Khumbu Glacier in relation to the Pyramid meteorological station and the Pheriche discharge station. Estimated ice thickness according to Huss & Farinotti (2012) is shown over the Khumbu Glacier together with the radio-echo sounding transects (black lines) of Gades et al. (2000) that was used to constrain thickness estimates.

The Cryosphere Discuss., doi:10.5194/tc-2016-116, 2016
Manuscript under review for journal The Cryosphere
Published: 16 June 2016

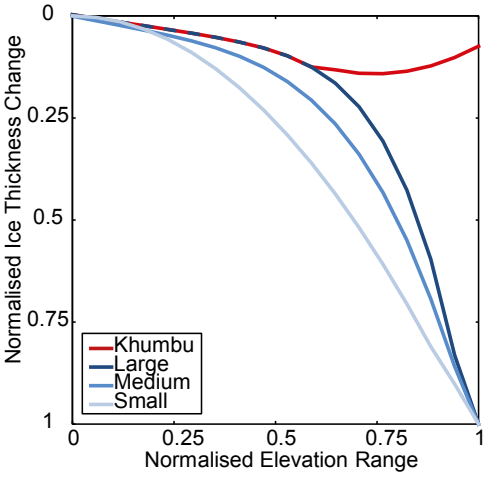

Figure 2: Δh-retreat parameterisation curves. 'Khumbu' is based on geodetically surveyed mass change in Nuimura et al. (2012), whereas curves for large, medium and small glacier are from Huss et al. (2010) based on various size classes of valley glaciers in the European Alps. The difference between the Khumbu and generic curves represents the stagnation and downwasting observed at Khumbu, with thickness changes near the terminus curtailed to prevent rapid terminus recession.

The Cryosphere Discuss., doi:10.5194/tc-2016-116, 2016
Manuscript under review for journal The Cryosphere
Published: 16 June 2016

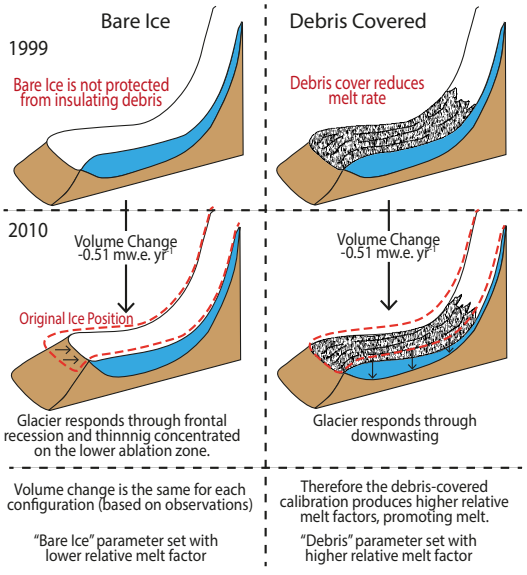

Figure 3: Schematic representation of the separate model configurations used for the calibration. 'Bare Ice' and 'Debris Covered' must both reproduce the same observed volume change, however, the parameter sets are different due to the presence or absence of the insulating debris layer.

The Cryosphere Discuss., doi:10.5194/tc-2016-116, 2016
Manuscript under review for journal The Cryosphere
Published: 16 June 2016

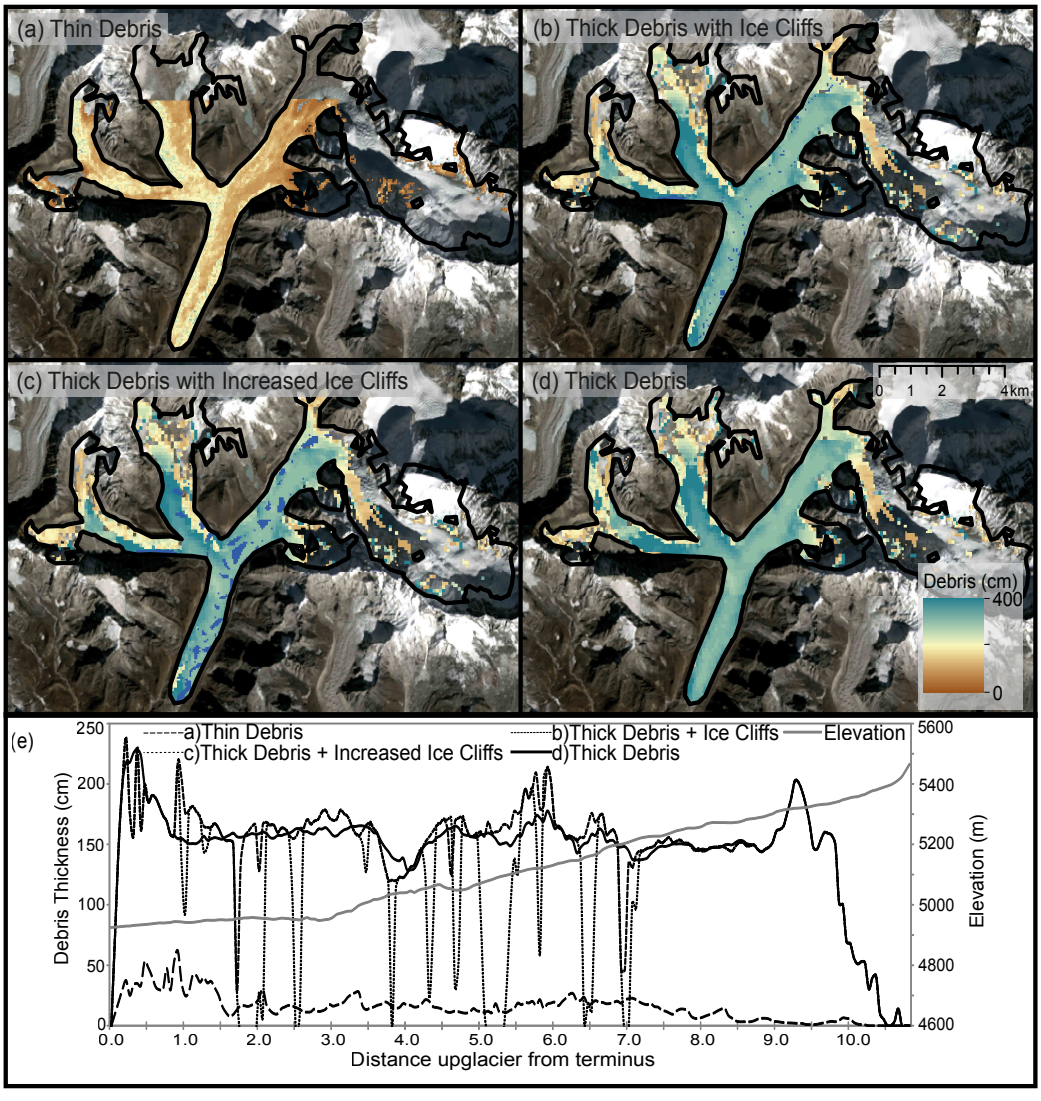

Figure 4: A comparison between the different debris surfaces used in this study. (a) is based on remote sensing and is provided by Rounce and Mckinney (2014). (b) to (d) are based on the modelled debris thickness of Rowan et al. (2015) with (d) showing modelled debris without modification, whereas (b) and (c) have been modified to include varying degrees of ice-cliff/melt-pond features; the proportion of features in (b) is based on current supraglacial ponds, whereas (c) shows enlarged features to mimic increased debris break-up. (e) is a comparison of aforementioned surfaces along 30m swath averaged around the central flowline. Elevation (solid grey line) is included.

The Cryosphere Discuss., doi:10.5194/tc-2016-116, 2016
Manuscript under review for journal The Cryosphere
Published: 16 June 2016

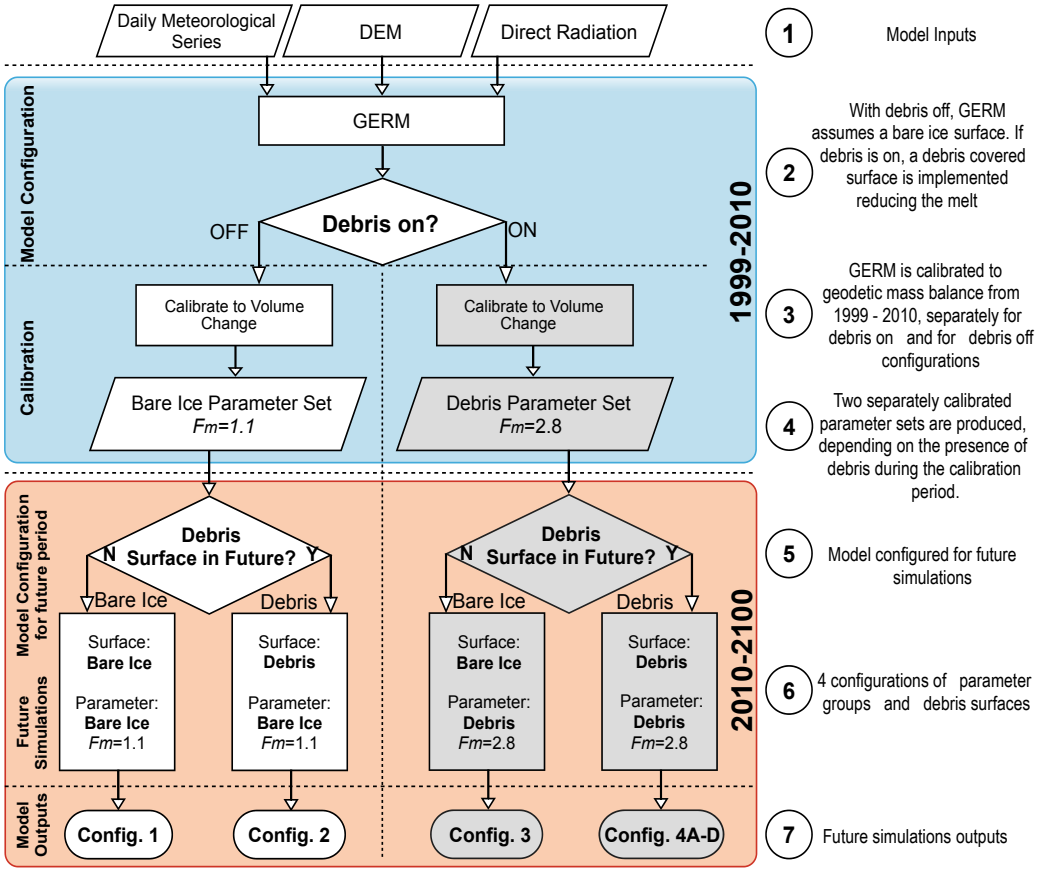

Figure 5: Flow chart showing (1) model inputs; (2) model configurations for the calibration period; (3-4) calibration process; (5-6) model configuration for the future simulations; (7) outputs for each separate configuration.

The Cryosphere Discuss., doi:10.5194/tc-2016-116, 2016
Manuscript under review for journal The Cryosphere
Published: 16 June 2016

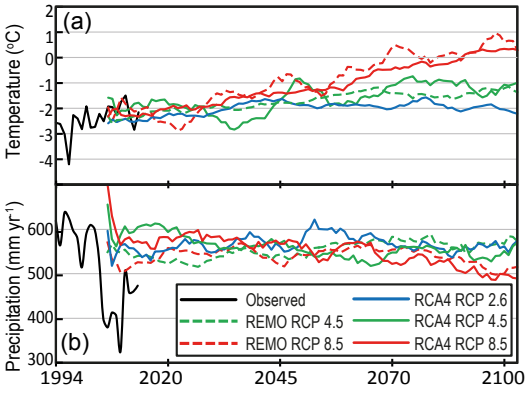

Figure 6: Corrected temperature (a) and precipitation (b) for RCP 2.6/4.5/8.5, with observed temperature from 1994-2010. RCPs show 10-year moving average, observed shows raw data.

The Cryosphere Discuss., doi:10.5194/tc-2016-116, 2016
Manuscript under review for journal The Cryosphere
Published: 16 June 2016

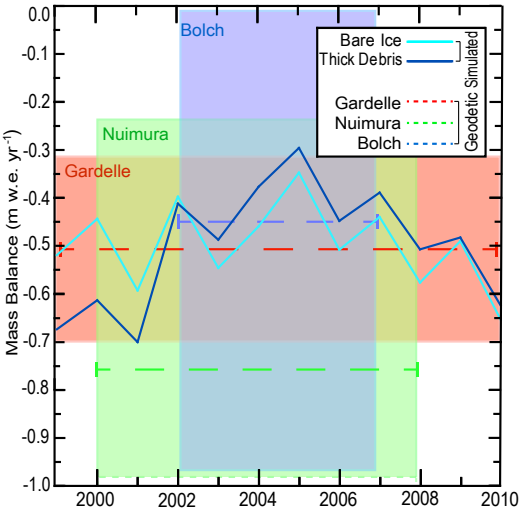

Figure 7: Simulated mass balance during the 1999-2010 calibration period, for the two model configurations. The dashed red line represents the geodetic mass balance from Gardelle et al. (2013), to which the model is calibrated from 1999-2010. Also included are the geodetic mass balance surveys of Bolch et al. (2011) and Nuimura et al. (2012), with the width of the lines representing the duration of study. Coloured boxes represent the uncertainty associated with each survey. Nuimura et al. (2012) lower bound of uncertainty is curtailed.

The Cryosphere Discuss., doi:10.5194/tc-2016-116, 2016
Manuscript under review for journal The Cryosphere
Published: 16 June 2016

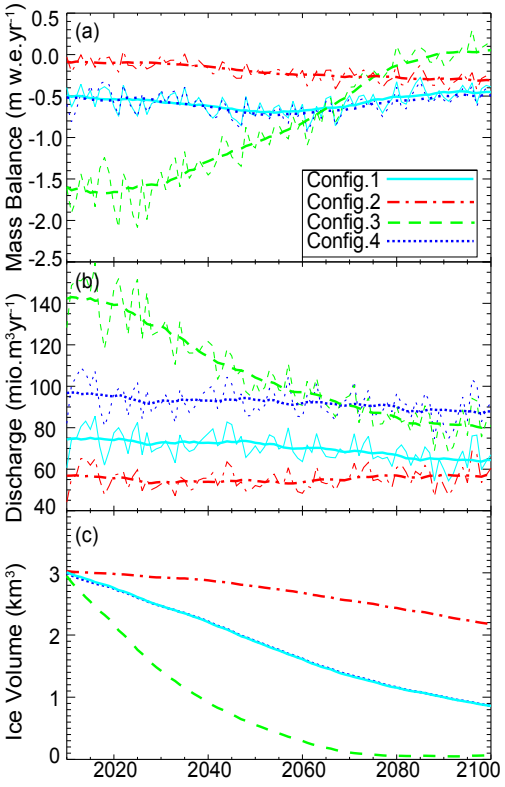

Figure 8: Evolution of (a) mass balance, (b) annual discharge, and (c) ice volume for different model configurations (see Fig. 5). Configurations: (1) bare-ice parameter set with bare ice surface; (2) bare-ice parameter set with thick debris surface; (3) thick debris parameter set with bare ice surface; (4A) thick debris parameter set with thick debris surface. Climate input for all simulations is bias-corrected RCP 4.5 scenarios from RCA4. Configurations 1 and 4 represent the calibrated model configurations, whereas 2 and 3 represent the addition/subtraction of debris surface to indicate model sensitivity.

The Cryosphere Discuss., doi:10.5194/tc-2016-116, 2016
Manuscript under review for journal The Cryosphere
Published: 16 June 2016

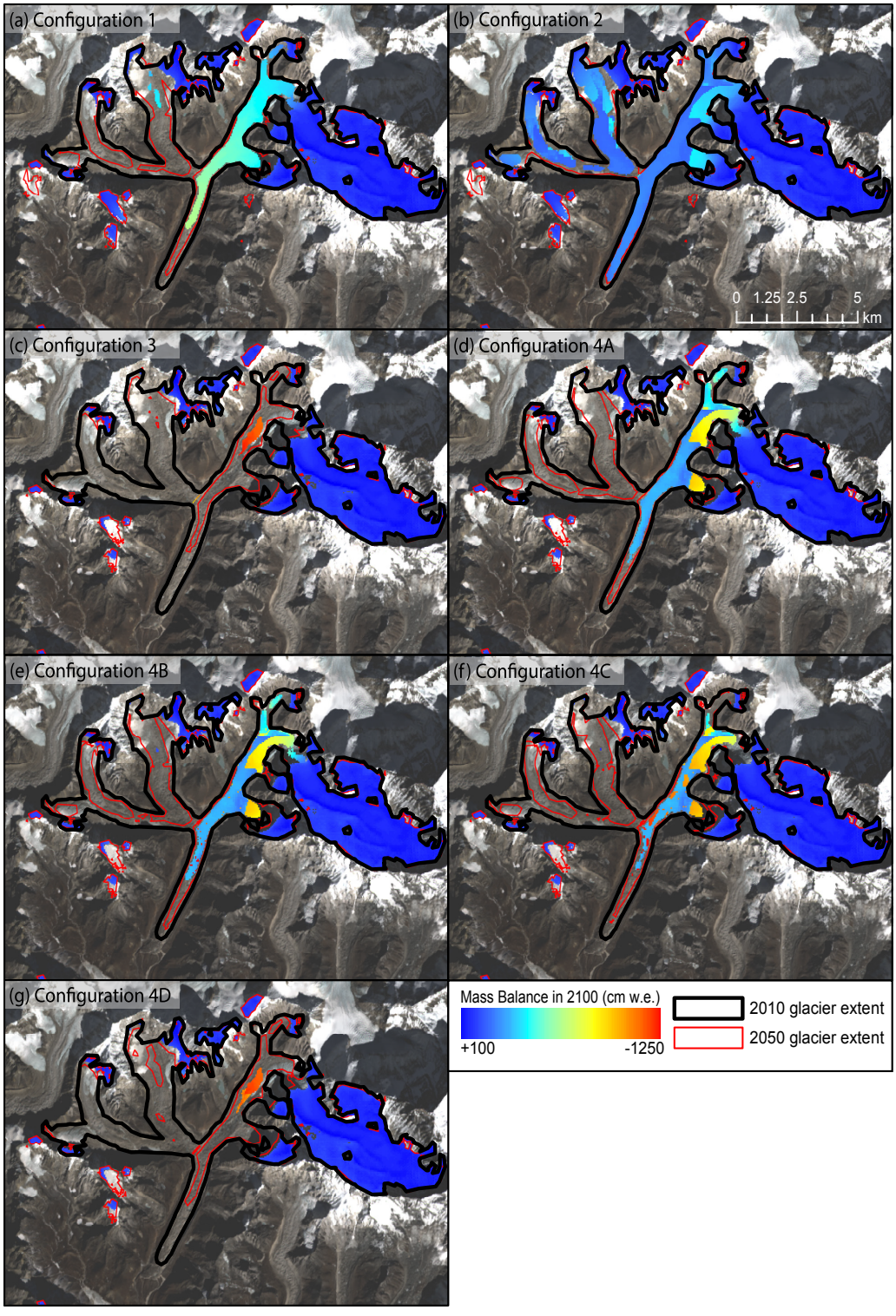

Figure 9: Modelled glacier extent in 2010, 2050 and 2100 with distributed mass balance in 2100 for each model configuration. The distinct steps in mass balance below the ice fall occur at the divide between debris-covered and clean ice.

The Cryosphere Discuss., doi:10.5194/tc-2016-116, 2016
Manuscript under review for journal The Cryosphere
Published: 16 June 2016

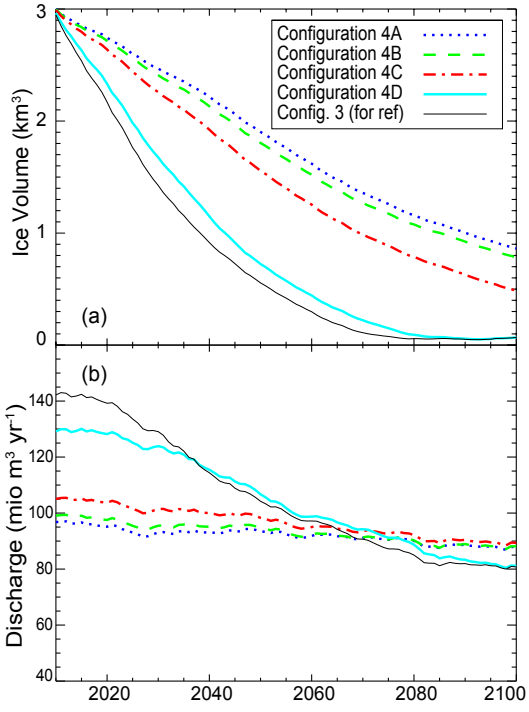

Figure 10: (a) Simulated ice volume and (b) simulated discharge, for differing debris surfaces. Volume loss increases with debris disintegration. The thin debris layer (4D) shows minimal insulation compared to bare ice, configuration 3, which is included for reference. Discharge is much higher where the ice surface is poorly insulated (4D and 3) until around 2070 after which the limited remaining ice volume results in overall lower discharge.

The Cryosphere Discuss., doi:10.5194/tc-2016-116, 2016
Manuscript under review for journal The Cryosphere
Published: 16 June 2016

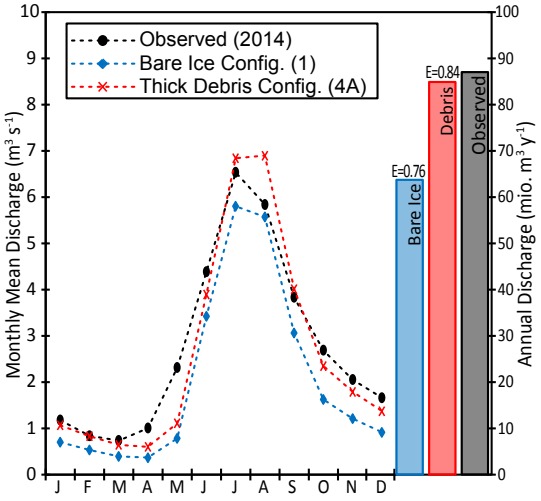

Figure 11: Simulated monthly discharge over the calibration period (1999-2010) for *bare ice* and *thick debris* configurations. Observed discharge at Pheriche during 2014 included for assessment of model performance. Columns represent total annual discharge. *E* refers to the Nash-Sutcliffe model efficiency.

The Cryosphere Discuss., doi:10.5194/tc-2016-116, 2016
Manuscript under review for journal The Cryosphere
Published: 16 June 2016

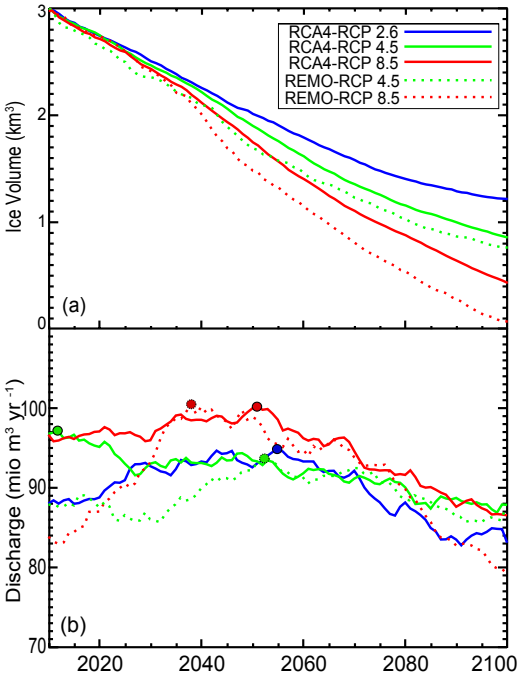

Figure 12: Evolution of (a) glacier volume, and (b) annual discharge, using model configuration 4 (thick debris). Two RCMs of the CORDEX-South Asia domain are used (RCA4 and REMO), with three RCPs from RCA4 (2.6, 4.5, 8.6) and two RCPs from REMO (4.5, 8.5) used to provide a range of scenarios. Thick black line on (b) is the mean linear trend of all simulations, and coloured circles represent peak discharge for respective simulation.